

TABLE 1

ID	RA(2000)	DEC(2000)	B	V	R	I	K	z_{min}	z_{phot}	z_{max}	χ^2_{ν}
72	12.088434	-7.71920	24.88	24.18	22.68	22.05	19.26	0.55	0.65	0.65	0.9
140	12.088446	-7.71231	24.31	24.19	23.54	23.30	20.28	1.20	1.30	1.40	0.9
89	12.088457	-7.71772	24.82	24.76	24.40	24.13	21.50	0.45	0.75	0.85	0.1
62	12.088474	-7.72053	24.84	24.66	24.05	23.24	20.38	0.90	1.10	1.25	0.1
285	12.088487	-7.69842	24.56	24.22	23.73	23.35	20.85	1.95	2.30	2.55	0.3
295	12.088511	-7.69778	23.92	23.15	22.61	22.34	21.50	0.30	0.40	0.45	1.0
307	12.088528	-7.69604	24.82	24.58	24.65	24.40	21.50	0.05	0.15	0.45	0.1
192	12.088536	-7.70709	25.04	24.63	23.74	23.27	20.91	0.50	0.60	0.75	0.1
122	12.088539	-7.71437	25.06	25.04	24.30	24.22	21.50	0.55	0.65	0.75	0.2
134	12.088548	-7.71324	24.54	24.27	23.20	22.74	20.79	0.60	0.70	0.70	0.2
312	12.088592	-7.69526	22.95	22.59	21.84	21.10	99.00	0.70	0.80	0.85	0.1
64	12.088599	-7.72003	25.12	24.88	24.71	24.59	21.50	1.20	2.55	3.00	0.1
296	12.088605	-7.69744	25.09	24.80	23.86	23.12	19.78	1.05	1.15	1.15	0.6
157	12.088610	-7.71073	25.02	24.41	23.35	23.14	20.86	0.45	0.55	0.65	0.5
242	12.088612	-7.70162	24.14	23.83	23.16	22.50	20.11	0.65	0.75	0.90	0.1
46	12.088617	-7.72350	22.93	21.76	20.89	20.44	18.12	0.10	0.35	0.40	0.2
309	12.088625	-7.69573	26.59	25.25	24.20	23.63	99.00	0.10	0.40	0.55	0.1
321	12.088639	-7.69416	24.66	24.61	24.01	23.50	99.00	0.65	0.80	0.85	0.1
31	12.088640	-7.72491	24.83	24.83	23.65	23.24	18.64	1.25	1.35	1.40	3.6
55	12.088650	-7.72128	25.28	25.44	24.51	24.62	21.27	2.05	2.25	2.40	1.7
270	12.088654	-7.69924	25.36	24.83	24.72	24.28	21.01	1.35	1.80	2.40	0.2
322	12.088665	-7.69388	25.30	25.57	24.60	23.61	99.00	0.85	1.10	1.15	0.9
113	12.088669	-7.71497	25.74	25.03	24.67	24.94	21.50	2.90	3.40	3.50	0.5
184	12.088695	-7.70742	24.42	24.18	23.43	23.33	21.50	0.45	0.55	0.70	0.3
109	12.088703	-7.71530	26.25	25.08	24.19	23.57	20.37	2.85	3.05	3.40	0.6
212	12.088752	-7.70463	23.29	22.96	22.32	21.62	19.44	0.70	0.80	0.90	0.1
236	12.088752	-7.70201	25.57	25.52	24.61	24.88	21.50	0.50	0.60	0.70	1.0
338	12.088767	-7.69233	24.91	24.77	24.40	23.77	99.00	0.75	1.15	1.60	0.0
130	12.088779	-7.71372	25.28	25.41	24.61	24.32	21.50	0.55	0.70	0.80	0.3
110	12.088791	-7.71520	24.95	24.76	24.23	23.60	21.50	0.70	0.80	0.90	0.1
258	12.088798	-7.70017	26.08	25.27	24.93	24.15	21.50	0.80	1.10	1.25	0.4
76	12.088802	-7.71854	25.09	24.87	24.19	23.71	21.50	0.50	0.70	0.80	0.1
299	12.088818	-7.69657	25.44	25.06	24.46	23.75	21.05	0.75	0.85	1.20	0.1
279	12.088828	-7.69844	24.95	24.86	24.68	24.10	21.50	0.80	1.10	1.80	0.1
67	12.088829	-7.71976	25.19	25.22	24.78	25.00	21.50	0.45	0.60	0.80	0.4
280	12.088838	-7.69814	25.29	24.82	24.55	23.83	20.54	1.10	1.55	1.90	0.2
98	12.088841	-7.71634	26.45	25.44	24.44	24.25	21.50	0.35	0.45	0.60	0.5
230	12.088861	-7.70257	24.00	23.65	23.05	22.48	20.14	0.65	0.75	0.85	0.1
247	12.088865	-7.70100	24.15	23.95	23.28	22.97	20.22	1.15	1.25	1.50	0.9
181	12.088883	-7.70755	24.76	25.00	24.38	23.94	21.50	0.70	0.80	0.85	0.5
166	12.088885	-7.70885	25.38	25.56	24.81	25.00	21.50	0.50	0.60	0.75	0.7
194	12.088897	-7.70620	25.15	24.94	24.32	24.25	21.50	0.45	0.55	0.70	0.1
13	12.088900	-7.72669	25.50	25.18	24.45	24.89	21.50	0.45	0.55	0.65	1.6
162	12.088915	-7.70989	25.03	24.89	24.01	23.43	21.14	0.60	0.75	0.80	0.3
268	12.088960	-7.69907	25.59	25.42	24.82	24.83	21.50	0.45	0.55	0.75	0.1

210	12.088999	-7.70451	24.18	24.00	23.67	23.85	21.50	0.35	0.45	0.55	0.8
308	12.089038	-7.69510	26.22	25.96	24.73	24.42	99.00	0.50	0.60	0.75	0.2
250	12.089040	-7.70060	26.22	25.54	24.08	23.41	19.08	1.05	1.15	1.15	3.8
149	12.089091	-7.71108	25.91	25.98	24.78	23.87	21.50	0.65	0.75	1.05	0.8
4	12.089102	-7.72698	25.30	25.29	24.40	23.78	21.50	0.60	0.75	0.85	0.3
301	12.089102	-7.69615	23.72	23.38	22.52	22.16	20.36	0.50	0.60	0.70	0.1
59	12.089105	-7.72024	25.22	25.09	24.45	23.73	20.02	1.20	1.30	1.45	0.1
178	12.089113	-7.70777	25.52	24.38	23.67	23.55	21.20	3.35	3.50	3.65	0.4
200	12.089149	-7.70535	25.15	25.32	24.63	23.91	21.50	0.75	1.10	1.20	0.5
49	12.089168	-7.72206	25.23	25.19	24.50	24.56	21.50	0.50	0.60	0.75	0.3
262	12.089189	-7.69949	25.79	25.19	24.44	23.76	21.50	0.40	0.75	0.85	0.1
119	12.089195	-7.71467	24.99	24.21	23.35	22.96	20.84	0.35	0.45	0.55	0.1
226	12.089229	-7.70285	25.45	24.94	24.37	24.17	21.50	0.05	0.45	0.60	0.1
259	12.089237	-7.69972	26.15	25.39	24.67	24.49	20.40	2.05	2.40	2.75	0.3
158	12.089255	-7.71024	26.38	25.49	24.67	24.28	21.50	0.10	0.45	0.60	0.1
300	12.089255	-7.69601	24.61	24.44	23.52	23.17	21.50	0.55	0.65	0.75	0.1
52	12.089320	-7.72122	26.06	25.09	24.87	24.44	21.50	2.60	3.00	3.50	0.1
95	12.089357	-7.71662	26.00	25.42	24.89	25.00	21.50	0.10	0.45	0.60	0.4
186	12.089362	-7.70677	24.57	24.24	23.85	23.61	21.16	1.90	2.25	2.60	0.1
287	12.089364	-7.69716	25.10	24.72	24.01	23.25	21.50	0.70	0.80	0.85	0.1
47	12.089370	-7.72216	26.45	25.32	24.05	23.74	21.50	0.35	0.45	0.60	0.6
238	12.089373	-7.70149	25.13	24.62	23.98	23.48	21.24	0.35	0.50	0.75	0.1
275	12.089379	-7.69839	25.89	24.44	23.20	22.55	19.51	0.35	0.45	0.55	0.5
136	12.089385	-7.71250	25.36	25.08	24.39	23.25	20.64	0.80	0.90	1.10	0.1
325	12.089387	-7.69275	23.51	23.08	22.47	21.98	99.00	1.20	1.35	1.60	0.1
53	12.089391	-7.72120	26.17	25.01	24.47	24.72	21.50	3.40	3.70	3.75	0.5
101	12.089410	-7.71620	23.77	23.21	22.50	22.25	20.49	0.40	0.50	0.55	0.1
61	12.089410	-7.71989	25.64	25.31	24.63	23.98	21.50	0.55	0.75	0.90	0.1
129	12.089434	-7.71358	25.36	25.22	24.44	25.00	21.50	0.45	0.55	0.70	2.0
203	12.089450	-7.70522	25.26	24.91	23.79	23.46	19.70	2.25	2.40	2.60	2.5
225	12.089470	-7.70267	25.20	24.82	24.45	25.00	21.50	2.05	2.30	2.60	1.5
320	12.089503	-7.69289	26.11	25.22	24.17	23.89	99.00	0.40	0.50	0.60	0.3
65	12.089506	-7.71972	25.17	25.31	24.54	23.89	21.50	0.70	0.80	0.85	0.5
54	12.089507	-7.72123	21.60	21.01	20.45	20.06	18.21	0.35	0.45	0.50	0.1
803	12.089554	-7.69767	26.32	24.80	23.57	22.42	18.82	0.75	0.85	0.85	1.3
273	12.089557	-7.69837	25.47	24.65	23.63	22.95	19.62	0.65	0.75	0.80	1.0
289	12.089557	-7.69685	25.03	24.30	23.45	23.31	21.31	0.40	0.50	0.55	0.5
94	12.089570	-7.71659	25.17	24.61	24.14	24.26	21.50	0.10	0.40	0.50	0.8
87	12.089581	-7.71743	26.14	25.10	24.40	24.30	21.50	3.30	3.50	3.80	0.3
239	12.089582	-7.70142	23.69	22.97	21.73	21.18	18.27	0.50	0.60	0.70	0.2
850	12.089582	-7.70506	24.95	24.46	24.14	24.43	21.50	2.80	3.20	3.30	1.2
311	12.089595	-7.69384	25.80	25.39	24.81	25.00	99.00	0.40	0.50	0.65	0.4
306	12.089600	-7.69454	25.00	24.84	24.71	24.31	21.50	0.75	1.70	2.65	0.1
206	12.089609	-7.70479	24.30	23.81	23.34	23.11	20.53	2.15	2.40	2.70	0.1
11	12.089619	-7.72536	22.09	21.19	20.41	20.00	17.86	0.30	0.40	0.50	0.1
79	12.089632	-7.71810	24.84	24.89	24.26	23.88	21.50	0.60	0.75	0.80	0.1
267	12.089637	-7.69866	25.35	24.77	23.32	22.53	19.69	0.60	0.70	0.70	0.6
323	12.089637	-7.69219	26.59	25.64	24.85	23.96	99.00	0.60	0.75	0.90	0.2
234	12.089639	-7.70146	24.99	24.97	24.45	24.03	21.50	0.55	0.75	0.85	0.1
851	12.089647	-7.70334	25.14	24.87	24.37	23.97	20.93	1.15	1.30	2.45	0.1
220	12.089654	-7.70298	25.50	25.04	24.16	23.61	20.41	2.25	2.50	2.70	0.8

263	12.089661	-7.69907	26.65	25.99	25.00	24.70	21.41	0.45	0.70	0.80	0.5
231	12.089691	-7.70182	25.92	25.71	24.55	24.31	21.50	0.55	0.65	0.70	0.3
328	12.089705	-7.69178	27.00	26.55	24.86	23.82	99.00	4.55	4.65	4.80	0.1
191	12.089706	-7.70657	25.20	24.89	24.05	23.75	21.50	0.50	0.60	0.75	0.1
20	12.089707	-7.72579	25.87	25.31	24.58	24.52	21.50	0.40	0.50	0.65	0.2
125	12.089709	-7.71393	24.71	24.41	24.08	23.64	21.08	1.15	1.35	2.20	0.1
219	12.089718	-7.70292	25.33	25.43	24.27	23.72	21.00	0.60	0.70	0.80	1.1
253	12.089724	-7.70009	22.98	22.83	22.45	22.13	19.85	1.15	1.25	2.35	0.2
335	12.089725	-7.69109	25.08	24.97	24.44	24.46	99.00	0.45	0.55	0.75	0.2
96	12.089726	-7.71649	24.90	25.09	24.34	24.04	21.50	0.60	0.75	0.80	0.4
305	12.089743	-7.69459	25.75	26.14	24.62	25.00	21.50	0.55	0.65	0.70	3.3
294	12.089767	-7.69662	25.17	24.46	23.66	23.02	19.22	1.10	1.20	1.30	0.9
190	12.089772	-7.70640	26.47	26.24	24.70	24.40	21.50	0.55	0.65	0.70	0.9
84	12.089776	-7.71761	25.55	25.88	24.80	24.01	21.50	0.75	0.85	0.85	1.2
283	12.089800	-7.69728	24.70	24.02	22.82	22.20	19.79	0.50	0.60	0.70	0.1
223	12.089808	-7.70270	26.96	25.70	24.08	22.99	20.14	0.55	0.65	0.65	0.4
209	12.089810	-7.70433	24.82	24.09	23.09	22.28	18.36	1.00	1.10	1.15	1.5
298	12.089872	-7.69587	24.82	24.11	23.07	22.11	18.88	0.65	0.75	0.90	0.1
240	12.089913	-7.70092	25.43	24.81	24.12	23.91	21.50	0.40	0.50	0.55	0.1
297	12.089921	-7.69594	25.76	25.09	24.65	24.41	20.82	1.80	2.35	2.75	0.1
123	12.089928	-7.71390	25.34	25.62	24.04	23.72	21.50	0.55	0.65	0.75	2.1
103	12.089950	-7.71566	26.79	25.60	24.47	23.81	21.50	0.30	0.50	0.65	0.1
233	12.089957	-7.70135	25.15	24.86	24.23	23.75	20.80	1.15	1.25	1.50	0.2
169	12.089966	-7.70831	25.44	25.04	24.48	24.66	21.50	0.35	0.45	0.65	0.6
108	12.089968	-7.71507	24.34	24.19	23.51	23.29	21.50	0.50	0.60	0.75	0.1
847	12.089979	-7.69428	25.11	24.07	23.17	22.55	99.00	0.30	0.40	0.50	0.1
177	12.089980	-7.70768	25.39	25.18	24.24	23.84	21.36	0.50	0.60	0.75	0.2
99	12.090004	-7.71621	24.82	24.84	23.68	23.76	21.50	0.55	0.65	0.70	2.2
333	12.090017	-7.69127	25.87	99.00	24.59	24.69	99.00	2.95	3.50	3.60	0.1
18	12.090031	-7.72600	25.14	24.84	24.09	23.62	21.50	0.45	0.70	0.80	0.1
183	12.090040	-7.70700	25.08	25.05	24.69	25.00	21.50	0.35	0.55	0.75	0.5
116	12.090048	-7.71472	24.78	24.30	23.68	23.61	21.50	0.35	0.45	0.60	0.3
319	12.090061	-7.69261	26.07	25.21	24.31	23.55	99.00	0.35	0.70	0.80	0.1
74	12.090067	-7.71861	23.41	22.89	21.98	21.23	18.60	0.65	0.75	0.85	0.1
249	12.090082	-7.70016	23.90	23.75	23.30	22.98	20.40	1.20	1.30	1.50	0.2
34	12.090094	-7.72441	24.29	23.49	22.71	22.44	20.70	0.35	0.45	0.50	0.2
276	12.090095	-7.69788	25.05	25.07	24.27	24.21	21.50	0.55	0.65	0.70	0.3
316	12.090116	-7.69292	25.12	24.76	24.16	24.15	99.00	0.40	0.50	0.65	0.2
215	12.090116	-7.70376	22.98	22.01	21.38	21.04	19.12	0.10	0.35	0.40	0.1
313	12.090144	-7.69310	26.57	25.52	24.97	24.88	99.00	2.75	3.45	3.75	0.1
213	12.090165	-7.70358	25.03	24.85	24.37	23.64	21.50	0.75	0.85	1.15	0.1
33	12.090206	-7.72439	25.02	24.77	24.21	23.84	20.55	1.20	1.35	1.70	0.2
164	12.090215	-7.70893	24.63	24.43	24.17	23.82	21.50	1.15	1.40	2.45	0.1
141	12.090238	-7.71166	24.71	24.11	23.71	23.56	21.50	0.10	0.40	0.45	0.1
216	12.090246	-7.70327	26.05	25.60	24.89	24.51	20.81	1.20	2.25	2.65	0.1
168	12.090279	-7.70846	24.62	24.26	23.78	23.69	20.71	2.05	2.25	2.60	0.3
274	12.090284	-7.69805	25.88	25.55	24.60	24.70	21.50	0.50	0.60	0.70	0.5
71	12.090337	-7.71924	22.89	22.39	21.59	20.96	18.45	0.55	0.75	0.80	0.1
185	12.090340	-7.70695	23.33	23.00	22.07	21.74	19.67	0.55	0.65	0.70	0.2
12	12.090340	-7.72685	27.00	24.72	23.67	22.85	21.50	4.55	4.65	4.70	0.3*

235	12.090358	-7.70151	25.55	24.82	23.49	22.85	19.55	0.55	0.65	0.70	0.6
56	12.090367	-7.72094	24.97	24.98	24.44	24.35	21.50	0.50	0.65	0.75	0.1
208	12.090367	-7.70451	25.35	24.89	23.90	23.47	21.50	0.50	0.60	0.70	0.1
172	12.090373	-7.70816	25.84	25.31	24.23	24.36	21.50	0.45	0.55	0.60	1.4
278	12.090375	-7.69749	25.03	24.85	24.29	24.01	20.95	1.15	1.30	1.65	0.3
179	12.090390	-7.70730	26.31	25.53	24.70	23.55	20.46	0.75	0.85	1.10	0.1
40	12.090402	-7.72350	24.81	24.61	23.86	23.54	20.52	1.20	1.30	1.50	0.8
50	12.090426	-7.72163	27.00	25.84	24.78	24.83	21.50	3.75	4.15	4.35	0.2
237	12.090429	-7.70125	24.76	24.56	24.03	23.64	21.11	1.15	1.25	1.60	0.2
248	12.090431	-7.70003	25.04	24.81	24.46	24.24	21.50	0.30	0.45	0.80	0.1
193	12.090453	-7.70621	27.00	26.76	24.82	24.61	21.11	3.95	4.15	4.25	0.3
852	12.090462	-7.70141	25.47	25.29	24.84	24.41	21.50	1.05	1.30	2.30	0.1
83	12.090485	-7.71806	26.14	25.92	24.91	24.45	21.50	0.50	0.70	0.75	0.1
82	12.090487	-7.71849	26.87	25.51	24.25	23.26	19.64	0.75	0.85	0.85	1.3
24	12.090527	-7.72558	25.73	25.20	24.13	24.02	21.50	0.45	0.55	0.70	0.5
92	12.090528	-7.71729	26.61	25.39	23.84	22.88	18.74	0.75	0.85	0.85	8.8
22	12.090550	-7.72595	25.69	25.27	24.61	23.78	20.20	1.05	1.15	1.30	0.1
128	12.090598	-7.71393	24.66	24.55	23.87	23.78	21.50	0.50	0.60	0.70	0.1
539	12.090622	-7.72455	25.44	24.86	24.04	24.13	21.50	0.40	0.50	0.60	0.8
73	12.090633	-7.71883	24.26	24.20	23.30	22.92	21.32	0.60	0.70	0.75	0.3
80	12.090661	-7.71831	25.38	25.34	24.00	23.30	19.88	1.00	1.15	1.15	1.4
540	12.090665	-7.72453	23.66	23.19	22.29	21.67	18.83	0.65	0.75	0.80	0.1
288	12.090685	-7.69643	26.37	26.39	24.61	24.38	21.50	0.55	0.65	0.70	1.8
143	12.090689	-7.71189	22.62	21.96	21.02	20.67	18.26	0.40	0.50	0.65	0.2
222	12.090716	-7.70302	23.58	23.26	22.52	21.84	19.49	0.65	0.80	0.85	0.1
609	12.090725	-7.71596	25.14	25.21	24.60	24.59	21.50	0.50	0.65	0.75	0.2
175	12.090731	-7.70788	27.00	26.14	24.82	24.33	21.50	3.70	4.40	4.60	0.1
211	12.090734	-7.70428	24.38	24.48	23.51	23.20	19.82	1.20	1.30	1.35	3.0
159	12.090742	-7.71021	25.12	24.68	23.86	23.62	21.50	0.45	0.55	0.65	0.1
224	12.090752	-7.70267	25.16	25.05	23.69	23.27	21.50	0.55	0.65	0.70	0.7
163	12.090754	-7.70956	24.32	24.18	23.61	23.39	20.57	1.20	1.30	1.50	0.7
608	12.090756	-7.71610	27.00	25.38	24.21	23.87	21.47	3.75	3.90	4.20	0.1
252	12.090799	-7.69989	24.31	24.36	24.05	23.78	21.50	0.55	0.75	0.90	0.1
111	12.090802	-7.71573	24.36	23.92	23.38	22.59	19.99	0.80	0.90	1.10	0.2
112	12.090806	-7.71530	24.88	24.16	23.55	23.07	20.78	0.10	0.40	0.50	0.1
38	12.090823	-7.72401	25.67	25.60	24.44	24.66	21.50	0.50	0.60	0.70	1.3
317	12.090825	-7.69298	24.91	24.75	23.70	23.68	99.00	0.50	0.60	0.70	0.7
27	12.090835	-7.72568	25.06	24.40	24.00	23.61	20.19	1.60	2.55	2.70	0.1
135	12.090848	-7.71300	25.80	26.00	24.36	23.84	21.50	0.55	0.65	0.75	1.8
30	12.090851	-7.72512	25.88	25.79	24.87	25.00	21.50	0.50	0.60	0.70	0.5

* probable star

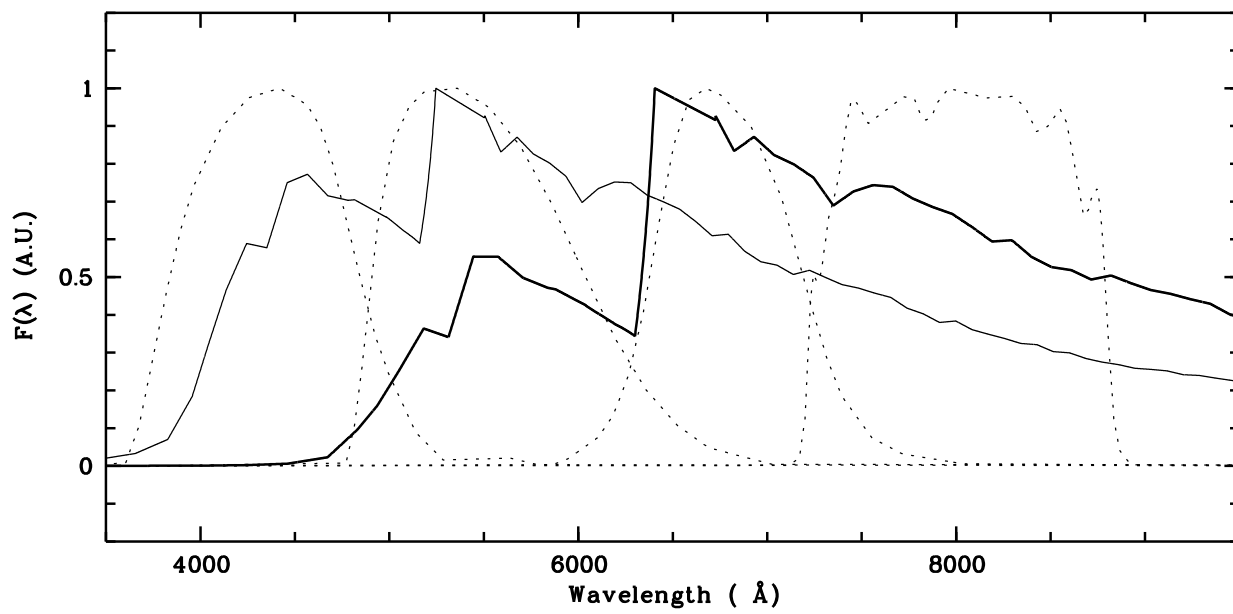


Table 2. Parameters Grid of Synthetic Spectra

	IMF	Scalo, Miller-Scalo, Salpeter
Exponential SFR Timescales (Gyr)		1,2,3,5,9, ∞ ,2 bursts
Age (Gyr)		.01,.05,.1,.25,.5,.75,1.,1.5,2., 3.,4.,5.,6.,7.,8.,9.,10.,11.,12.
Metallicities		Z_{\odot} , $0.2Z_{\odot}$, $0.02Z_{\odot}$
E_{B-V}		0,0.03,0.06,0.1,0.2,0.3
Extinction Law		Calzetti

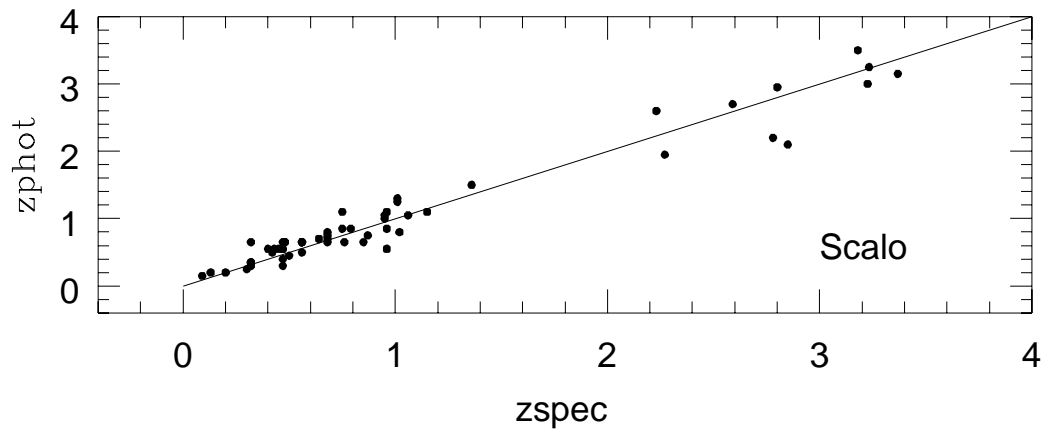
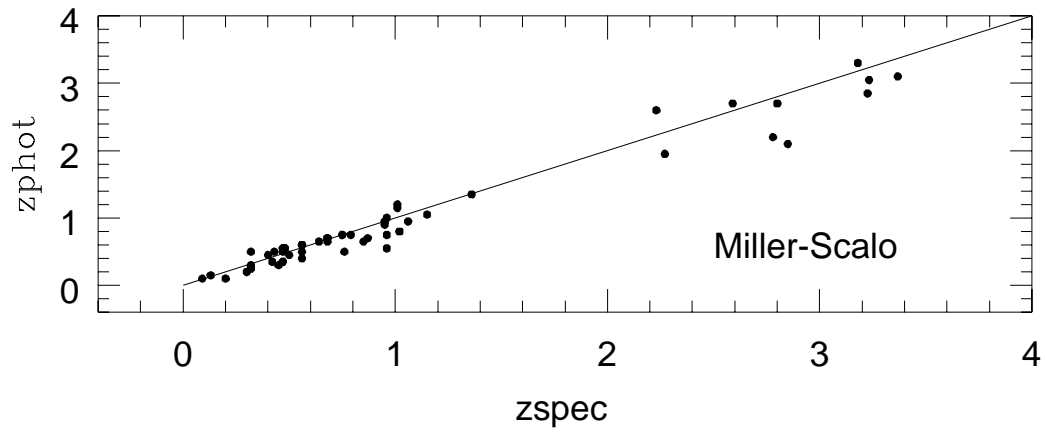
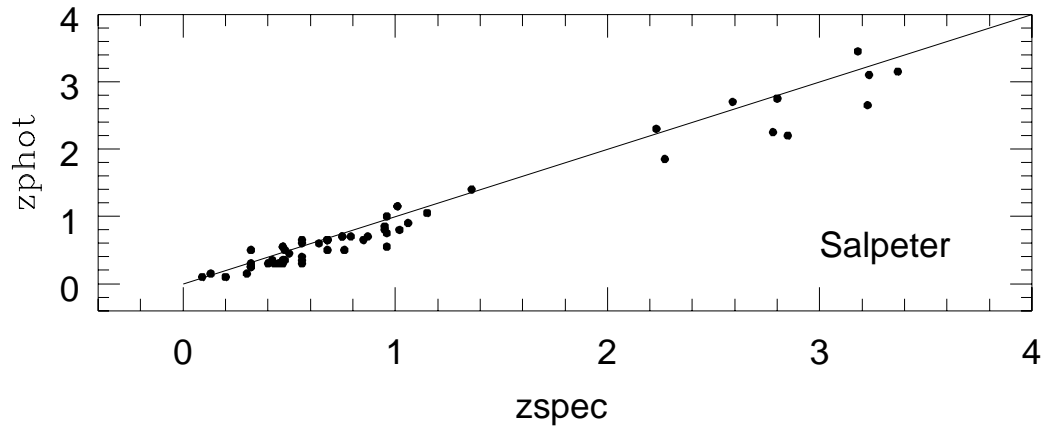
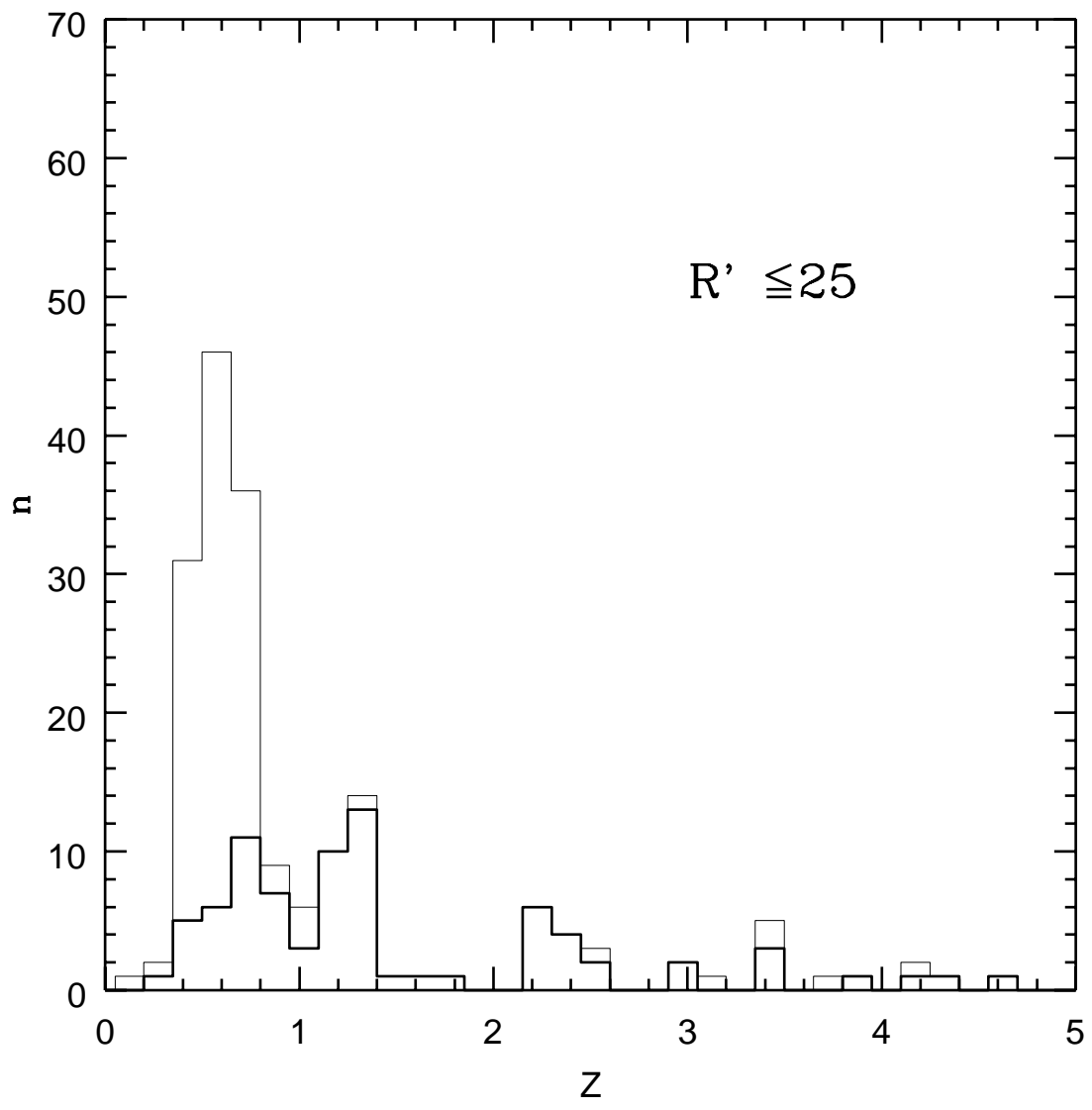


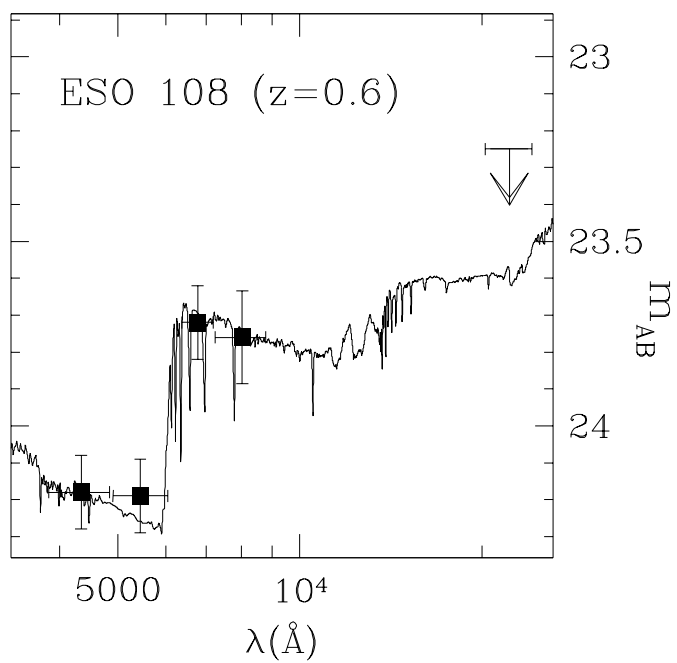
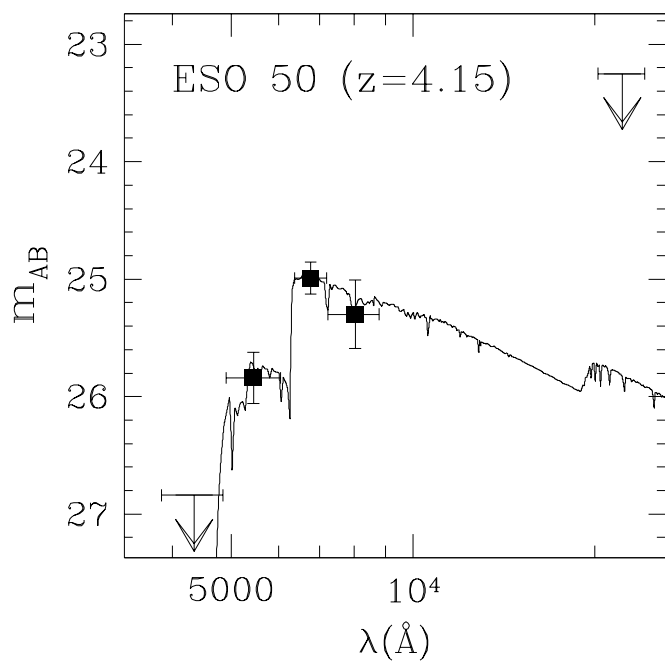
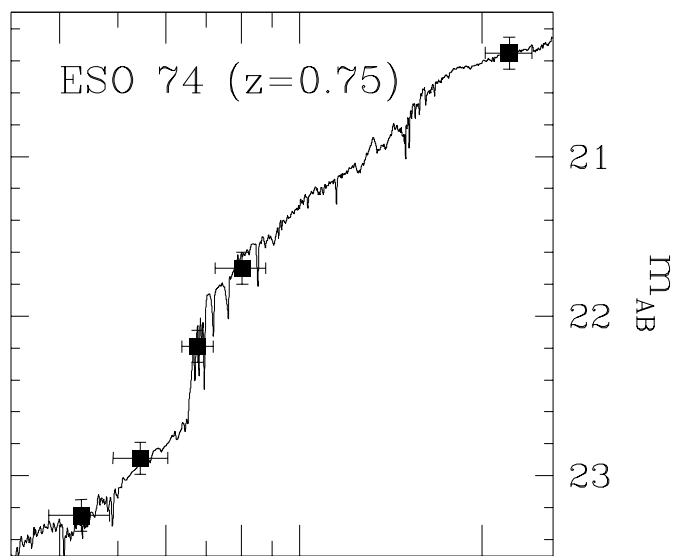
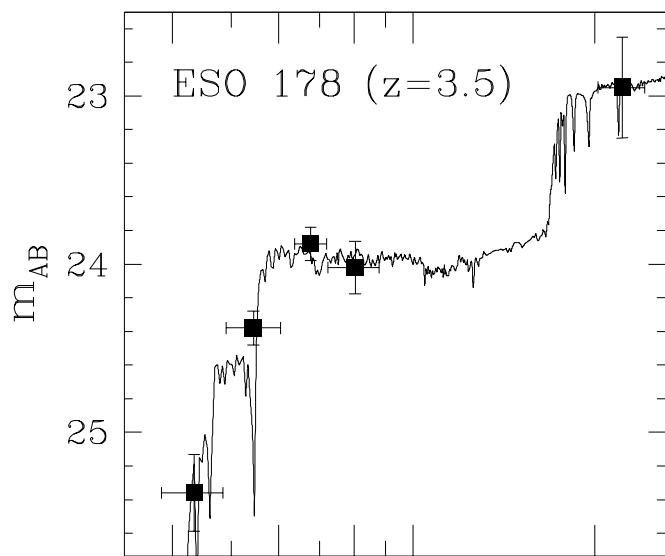
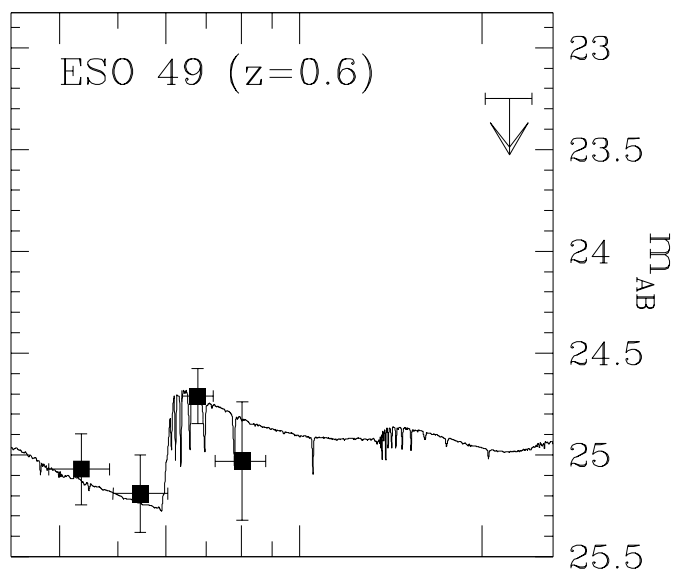
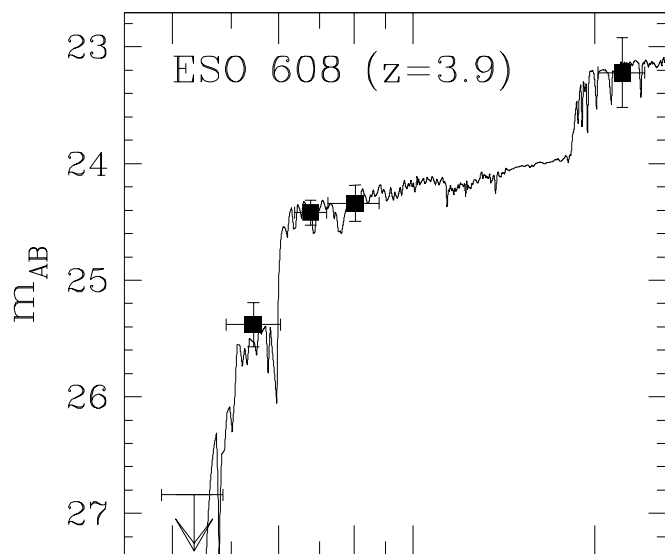
Table 3. Comoving Luminosity Density from the $R' \leq 25$ sample

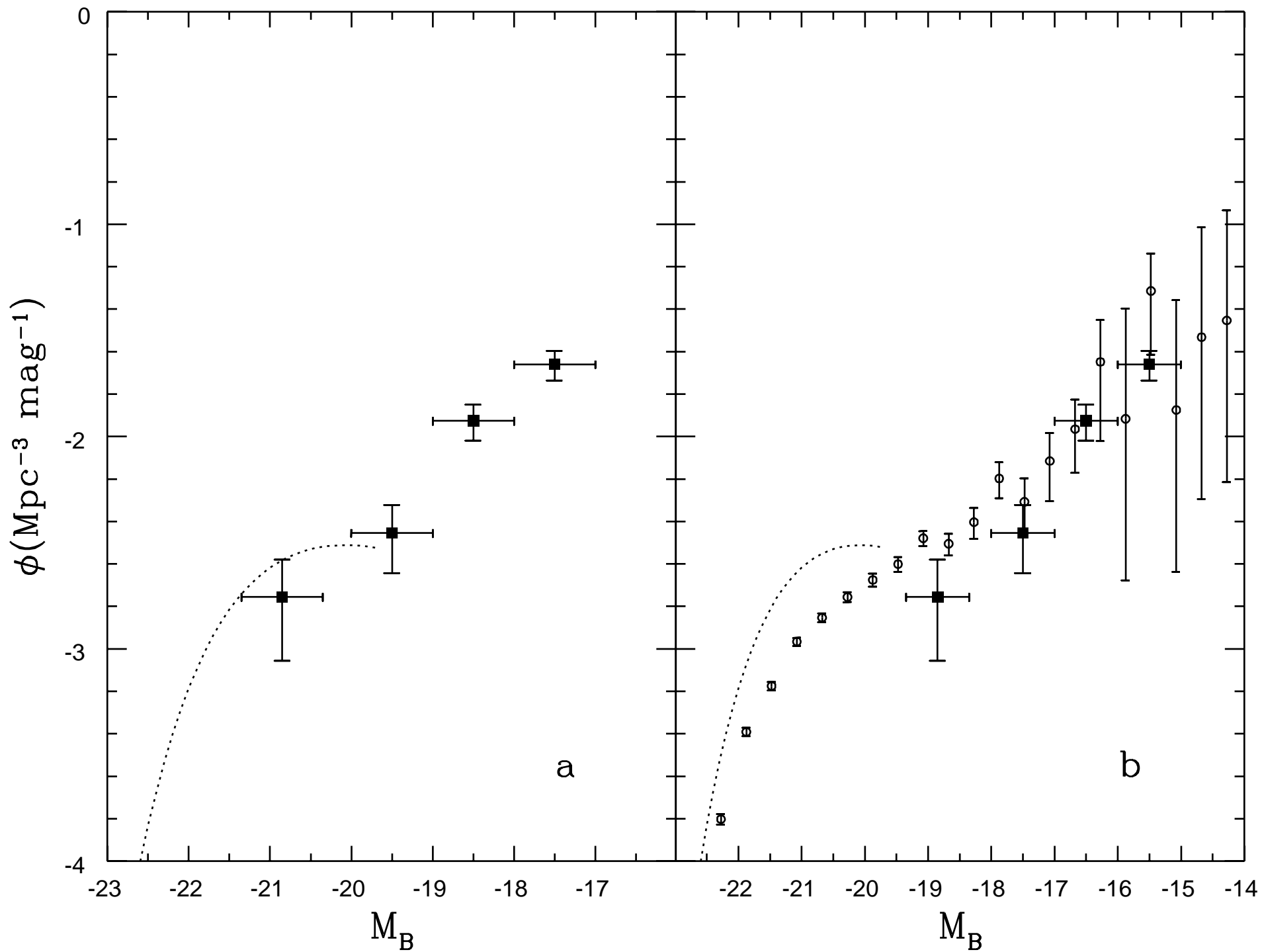
z	Observed ^a	Uncertainties
0.15 ^b	18.90	0.16
0.375	19.09	0.08
0.575	19.23	0.06
0.825	19.26	0.05
1.25	19.17	0.07
2.75	18.95	0.09
4	18.97	0.13

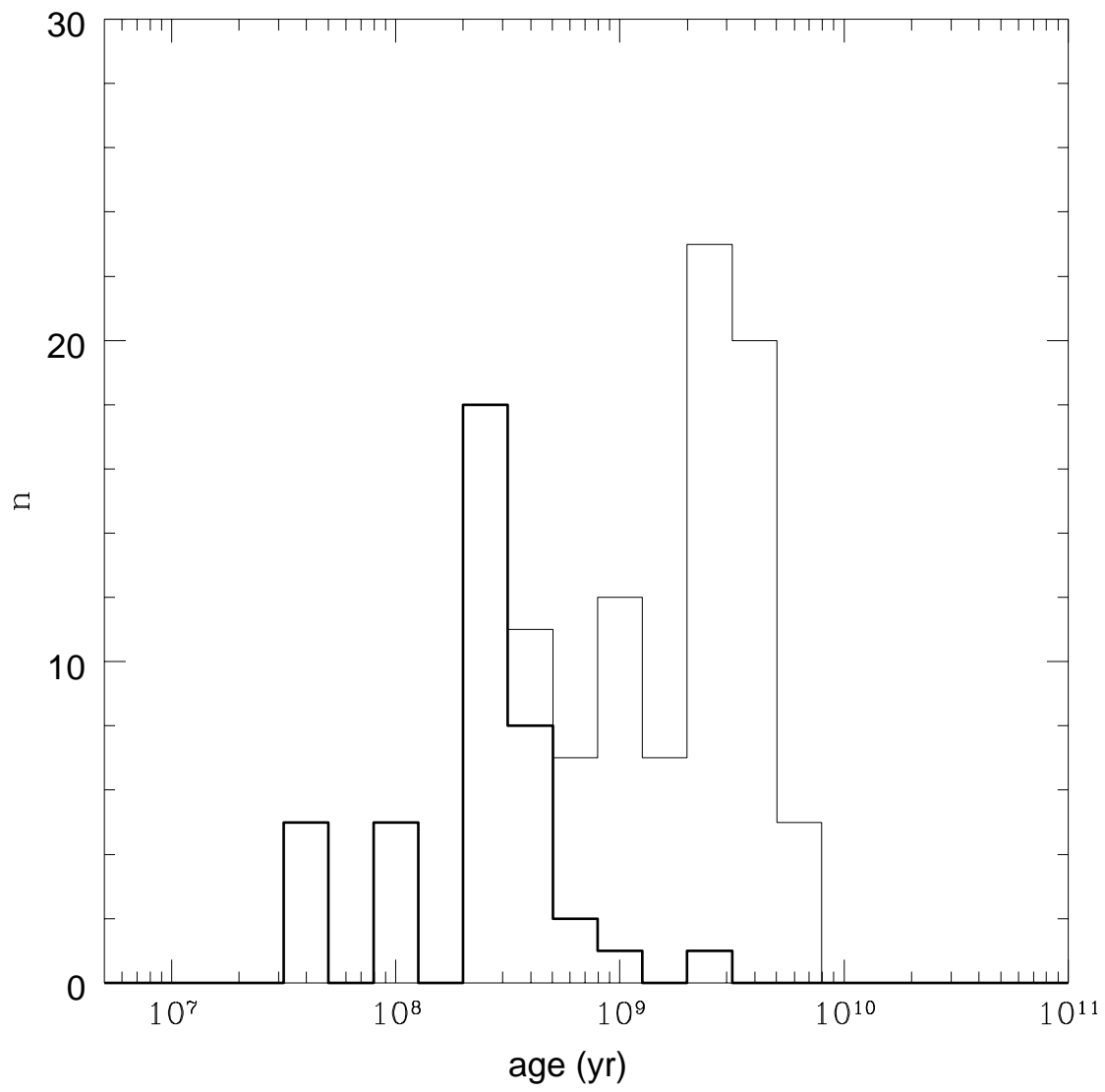
^a $\log L$ (2800 Å) W Hz⁻¹ Mpc⁻³

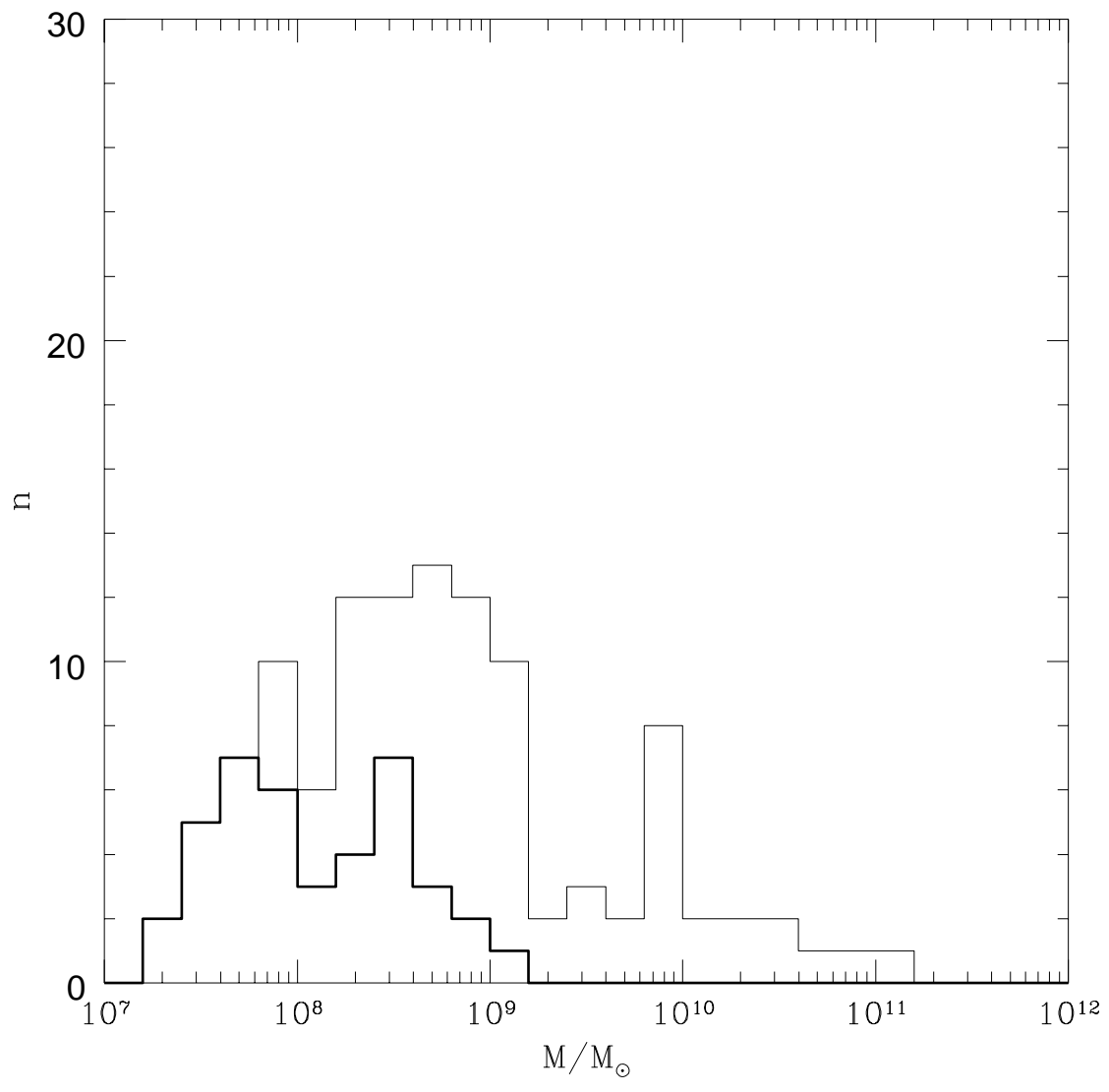
^b The local value is from Treyer et al. (1997)

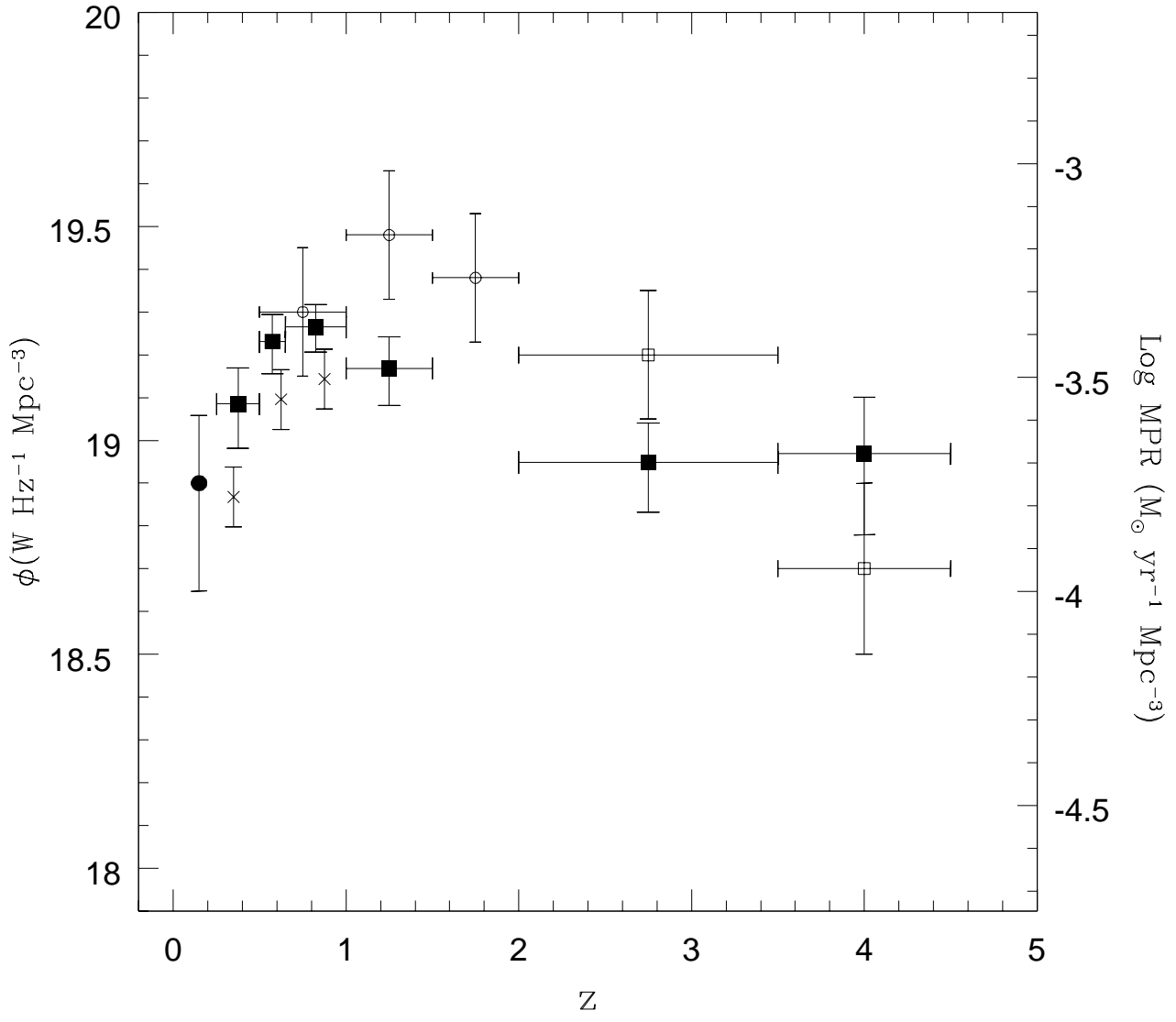


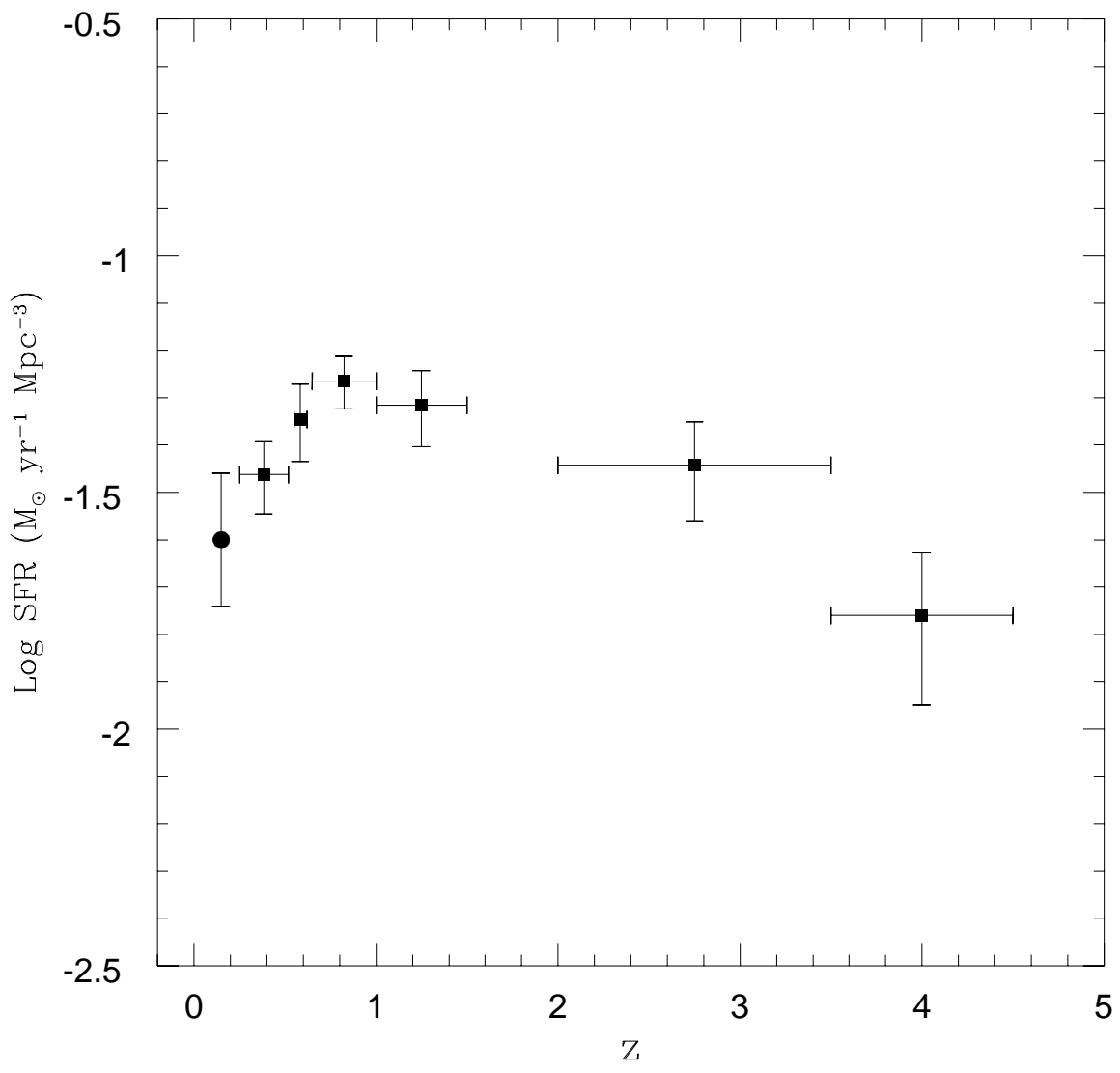


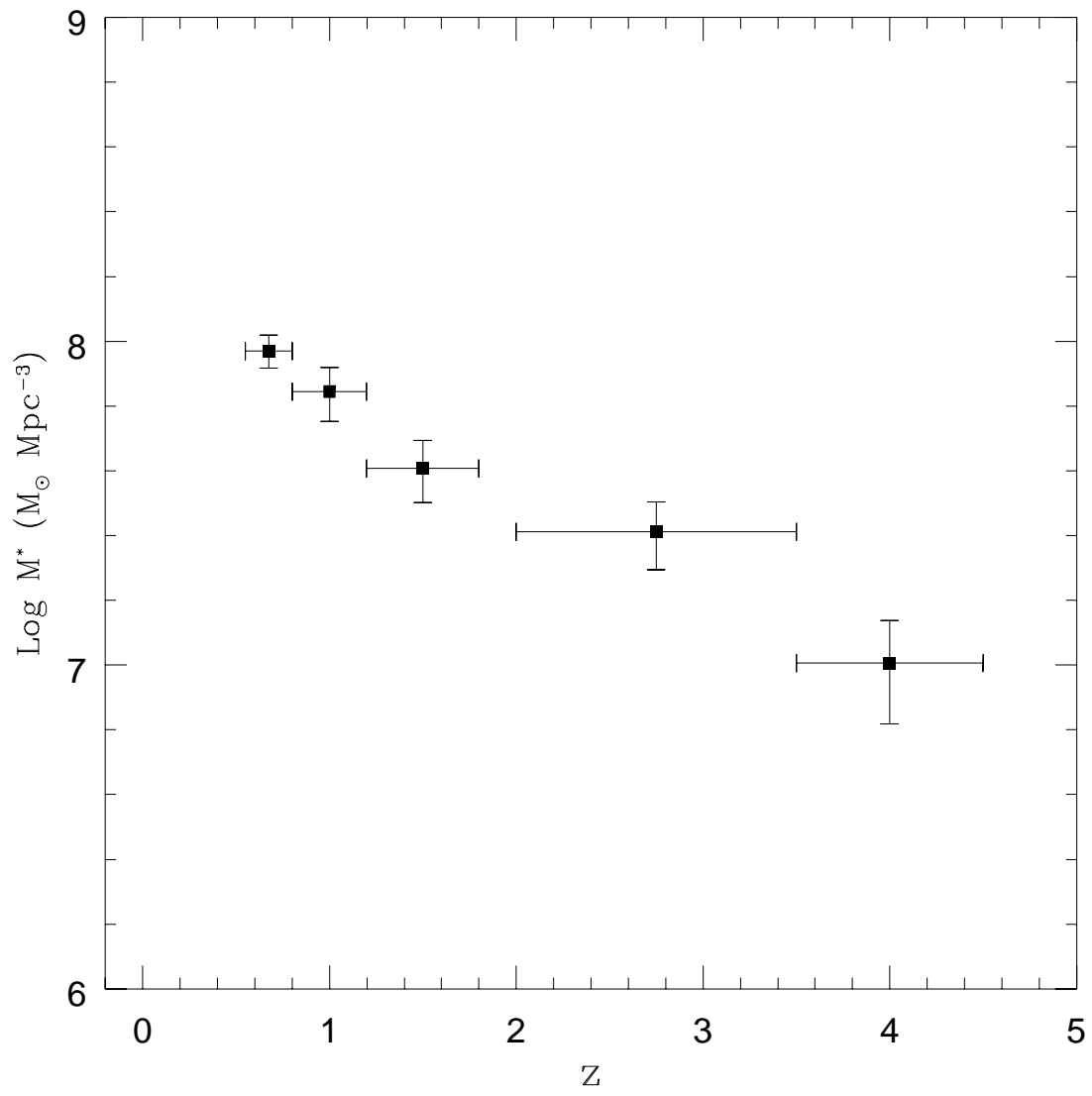












THE PHOTOMETRIC REDSHIFT DISTRIBUTION AND EVOLUTIONARY PROPERTIES OF GALAXIES UP TO $z \sim 4.5$ IN THE FIELD OF THE QUASAR BR1202-0725 ¹

E. Giallongo¹, S. D'Odorico², A. Fontana¹, S. Cristiani³,
E. Egami⁴, E. Hu⁵, R. G. McMahon⁶,

¹ Osservatorio Astronomico di Roma, via dell'Osservatorio, I-00040 Monteporzio, Italy

² European Southern Observatory, Karl Schwarzschild Strasse 2, D-85748 Garching, Germany

³ Dipartimento di Astronomia, Università di Padova, vicolo dell'Osservatorio 5, I-35122, Padova, Italy

⁴ MPE, Postfach 1603, D-85740 Garching, Germany

⁵ Institute for Astronomy, University of Hawaii, 2680 Woodlawn Dr., Honolulu, HI 96822, USA

⁶ Institute of Astronomy, Cambridge CB3 0HA, UK

arXiv:astro-ph/9802340v1 26 Feb 1998

¹Based on observations collected at the NTT 3.5m of ESO and at UH 2.2m of the Hawaii

ABSTRACT

We present a deep BVrIK multicolor catalog of galaxies in the field of the high redshift ($z = 4.7$) quasar BR 1202-0725. Reliable colors have been measured for galaxies selected down to $R = 25$. Taking advantage of the wide spectral coverage of the galaxies in the field, we compare the observed colors with those predicted by spectral synthesis models including UV absorption by the intergalactic medium and dust reddening. The choice of the optical filters has been optimized to define a robust multicolor selection of galaxies at $3.8 \leq z \leq 4.5$. Within this interval the surface density of galaxy candidates with $z \sim 4$ in this field is 1 arcmin^{-2} . Photometric redshifts have been derived for the galaxies in the field with the maximum likelihood analysis using the GISSSEL library of $\sim 10^6$ synthetic spectra. The accuracy of the method used has been discussed and tested using galaxies in the Hubble Deep Field (HDF) with known spectroscopic redshifts and accurate photometry. A peak in the redshift distribution is present at $z \simeq 0.6$ with relatively few galaxies at $z > 1.5$. At variance with brighter surveys ($I < 22.5$) there is a tail in the distribution towards high redshifts up to $z \sim 4$. The luminosity function at $z \sim 0.6$ shows a steepening for $M_B > -19$. This increase is reminiscent of that found in the most recent estimates of the local luminosity function where a similar volume density is reached about 2 mag fainter. The observed cosmological ultraviolet luminosity density is computed in the overall redshift interval $z = 0.3 - 4.5$ reaching a value $\sim 2 \times 10^{19} \text{ W Hz}^{-1} \text{ Mpc}^{-3}$ at $z \sim 0.8$. Including recent local estimates it appears that the UV luminosity density changes by a factor ~ 2.5 in the overall redshift interval $z = 0.1 - 4$, not including correction for fainter undetected galaxies. Thus we find that the evidence of a marked maximum in the luminosity density at $z \sim 1 - 1.5$ for galaxies with $R \leq 25$ is weak. We have derived in a homogeneous way, using the GISSSEL libraries, the physical parameters connected with the fitted spectral energy distributions. Thanks to this new approach, the problem of the star formation history of the universe is dealt with in a self consistent way taking into account the dust and metallicity distributions derived from the spectrophotometric properties of each galaxy in the sample. The bulk of the blue intermediate redshift population with $z = 0.4 - 1$ mostly consists of very young star-forming galaxies with a median starburst age of the order of a few 10^8 yr and typical mass in luminous stars $\sim 2 \times 10^8 M_\odot$. The presence of this young population is in contrast with pure luminosity evolutionary model (PLE) based on a single high formation redshift. The cosmological mass in formed stars per unit comoving volume at $z \sim 3$ is already $\sim 20\%$ of that formed at $z = 0.5$ in our magnitude limited sample. Predictions based on the standard hierarchical clustering models are smaller, although not far from that derived from the observations.

Key words : galaxies: evolution

1. INTRODUCTION

Deep photometric and spectroscopic surveys of galaxies performed by means of large ground-based telescopes and the HST are providing a first insight into the cosmological distribution of galaxies of different spectral types up to $z \sim 5$.

The bulk of the contribution to surveys of intermediate depth ($B < 24.5$, $I < 23$, and $K < 20$) comes from galaxies at redshifts $z \sim 0.5$ with a tail in the distribution extending up to $z \sim 1.5$ (Songaila et al. 1994, Lilly et al. 1995, Ellis et al. 1996, Cowie et al. 1996). These surveys show substantial evolution in the galaxy properties starting already at $z \geq 0.5$. The presence of massive star formation is provided by the observed blue colors of galaxies and by the detection of strong emission lines.

The recognition of the evolutionary path of the average star formation rate per unit comoving volume is one of the main tools to understand the processes that control the formation and evolution of galaxies in the universe. An increase by a factor of ten in the redshift interval $z = 0 - 1$ has been recently suggested (Lilly et al. 1996, Madau et al. 1996). This of course implies that about half of the stars formed at intermediate redshifts, in general agreement with theoretical expectations of CDM cosmologies. Nevertheless, the same cosmological scenarios predict a fraction $< 2\%$ of the present mass density in stars at $z > 4$ (Cole et al. 1994). It is therefore at these high redshifts that cosmological scenarios for galaxy formation are more vulnerable to observational constraints. Thus, the search and discovery of galaxies at $z > 2$ is a major challenge of recent observational cosmology.

Until recently, however, these objects have proven to be quite elusive, being detected neither in complete spectroscopic surveys limited to $I \leq 22.5$, (Lilly et al 1995 CFRS, Cowie et al 1996), nor in field surveys based on the search of highly redshifted Ly α line emission (Thompson et al 1995) with some relevant exceptions (Macchetto et al. 1993, Warren and Møller 1996).

Quite recently, improved sensitivities and new observational strategies have led to the discovery of star-forming galaxies up to $z \sim 4.5$. Deep Ly α searches have been successfully tuned at particular redshifts, such as those of previously known quasars (Hu and McMahon 1996), radio galaxies (Pascarella et al 1996) or strong QSO absorption systems (Francis et al 1996). Deep multicolor searches are also proving very effective at detecting field galaxies in relatively wide redshift intervals. The technique based on the color selection of the Lyman break feature in flat spectrum star-forming galaxies has been

applied by Steidel and co-workers to look for field galaxies at $2.8 < z < 3.4$, (Steidel and Hamilton 1992, Steidel et al 1995), with a remarkable spectroscopic success rate of $\simeq 70\%$ (Steidel et al 1996). We have also applied a similar multicolor technique to look for the galaxies responsible for strong Ly α absorption in quasar spectra. By means of deep BVR images around the $z = 4.695$ quasar BR1202-0725 we discovered a galaxy companion whose redshift was estimated to be in the range $z \geq 4.4 - 4.7$ (Fontana et al. 1996) on the basis of sharp color criteria obtained comparing observed colors with that expected by star-forming galaxies once UV absorption by the intergalactic medium has been taken into account (Madau 1995). Narrow band imaging and spectroscopic follow up have confirmed the $z = 4.7$ redshift of the galaxy (Hu et al. 1996, Petitjean et al. 1996).

The majority of galaxies detected in the Hubble Deep Field (HDF; Williams et al. 1996) are too faint to be investigated by spectroscopy. The only way to derive statistical information about their cosmological distribution is based on color-estimated redshifts (Gwinn & Hartwick 1996, Lanzetta et al. 1996, Sawicki et al. 1997). The reliability of the method depends mainly on the number of colors used and on the modeling of the galaxy templates. The possibility to calibrate the color-estimated redshifts with fair samples of spectroscopic galaxies allows better accuracy (Koo 1985, Koo & Kron 1992, Connolly et al. 1995).

We have applied the “photometric redshift technique” to derive the redshift distribution of the complete galaxy sample in the field of the quasar BR1202-072 and the results are discussed in this work. To make the redshift estimates more robust we have extended the spectral coverage in the field adding deep K images ($K \simeq 21.5$ at 3σ sky limit). Photometric redshifts have been derived with a maximum likelihood analysis over the five broad bands BVR $\bar{I}K$ using a library of $\sim 10^6$ synthetic spectra. A calibration of the method has been carried out over about 60 galaxies in the HDF with known spectroscopic redshifts. In Sect. 2 we present the data sample, in Sect. 3 the library of galaxy synthetic spectra and our statistical technique for color-estimated redshifts. In Sect. 4 we describe our multicolor selection of galaxies with $z > 3.8$ and in Sect. 5,6 we describe and discuss the relevant results concerning the cosmological evolution of the galaxy properties.

2. THE DATA SAMPLE

The field of BR 1202-0725 was observed with the SUSI imaging CCD camera at the Nasmyth focus of the ESO New Technology Telescope. Four broad band filters were used during three photometric nights, 1995 April 23-36. Standard BVI passbands of the Johnson-Kron-Cousins system and Thuan-Gunn r system were used. Several dithered images were obtained in the four broad bands with total integration times of 15000, 10800, 7200, 7800 s for the BVI bands. The FWHM of the stellar images in the combined frames are 1, 1, 0.6, 0.65 respectively. This is better than most data of other deep surveys and it is an advantage for the accuracy of the photometry at the fainter magnitudes where the density of objects is high.

The photometric calibration was obtained from several standard stars observed on the same nights and at similar airmasses. Total magnitudes were obtained in an aperture of fixed size (1.8 arcsec), applying a seeing-dependent aperture correction.

We have calibrated $B'V'R'I'$ magnitudes in the “natural” system defined by our instrumental passbands. The zero points of our instrumental system were adjusted to give the same $BVRI$ magnitudes as in the standard system for stellar objects with $B - V = V - R = R - I = 0$. The colour transformation for stellar objects was $I' = I$, $B' - V' = 0.91 \times (B - V)$, $V' - R' = 1.17 \times (V - R)$, and $R' - I' = 0.74 \times (R - I)$. The magnitudes were corrected for galactic absorption, with $E(B - V) = 0.03$. Transformations to the AB systems give $I_{AB} = I' + 0.47$, $R_{AB} = R' + 0.21$, $V_{AB} = V'$, $B_{AB} = B' - 0.16$

The K band observations have been obtained at 2.2m telescope of the University of Hawaii in two runs: 15-17 April 1994 for a total of 10.4 h on the central 90×90 arcsec² field and 17-19 March 1995 with QUIRC 1024² array for a total of 7 hrs on a 3×3 arcmin² field encompassing the SUSI field.

A galaxy catalog has been extracted from the best quality image in the r band with the SExtractor image analysis package (Bertin & Arnouts 1996). To detect objects and compute total magnitudes we have followed the standard procedure described by Smail et al. (1995). We first smooth the frame with the point-spread function derived from stellar profiles in the field and then threshold it at a level of 2.2σ of the sky noise in the raw frame and identify objects. This threshold provides a detection of galaxies down to $R' = 25.8$.

Total magnitudes have been obtained using a fixed aperture (1".8 diameter or ≥ 3 FWHM) after an aperture correction to a 5" diameter under the assumption

that the objects have roughly stellar profiles, this results in an aperture correction of $\delta R' = 0.1$ at $R' \simeq 25$. The validity of the assumption has been tested in previous similar deep images (Smail et al. 1995).

For objects brighter than $R' = 23$, where isophotal diameters are larger than our fixed aperture, we adopted isophotal magnitudes. To measure colors for our objects we measure aperture magnitudes in all the bands in the same positions defined in the r frame with the appropriate aperture corrections. To put stringent limits on the galaxy colors we have adopted 2σ upper limits in the $B'V'I'$ bands of 27, 26.6, 25, respectively. Since the sky noise in the K image changes appreciably across the field, we have adopted the more conservative 3σ threshold $K = 21.5$.

In order to discuss the statistical spectral properties of faint galaxies we have computed reliable colors only for galaxies with $R' \leq 25$ for which the surface density in our field 1.4×10^5 deg⁻², in agreement with the results of Smail et al. (1995).

Coordinates (obtained using 11 APM stars as reference in the field) and magnitudes for all the galaxies selected in the interval $20 < R' < 25$ are shown in Tab. 1.

3. THE PHOTOMETRIC REDSHIFT TECHNIQUE

3.1. The Synthetic Spectral Libraries

To derive photometric redshifts for all the galaxies in the catalog we have computed the expected colors (in our photometric system) for galaxies as a function of the redshift using the spectral synthesis model (GISSEL library) by Bruzual & Charlot (1997). Models of this kind have a number of free parameters which control the spectral properties of different spectral types of present-day galaxies.

The UV flux emitted by galaxies is directly related to the star-formation rate of each galaxy. This is governed by the assumed e - *folding* star formation time-scale τ and by the age of the galaxy. Different combinations of ages and τ values result in different spectral types. For example, a star-formation timescale of $\tau \leq 1$ Gyr and an age ≥ 12 Gyr is more appropriate for an early type galaxy, while $\tau = 2, 4, 7$, Gyr or constant SFR fit well typical spectra of Sb, Sbc, Sc, or Irregulars respectively (Bruzual & Charlot 1993).

Although smooth star-formation rates declining with an exponential law can adequately represent the global star-formation history of most of the present day galax-

ies, there are observational hints and theoretical expectations for a star-formation history which shows signs of stochastic episode of starburst formation.

This situation can be parameterized in terms of the Scalo (1986) parameter b , defined as the ratio of the SFR at the current time to the past SFR averaged over the age of the galaxy. A constant or declining SFR of the kind $SFR \propto \exp(-t/\tau)$ gives always $b \leq 1$. In contrast, multiple bursts can lead to values of the Scalo parameter $b > 1$ as observed in a few local galaxies where $b = 1 - 5$ has been derived (e.g. Kennicutt, Tamblyn, & Congdon 1994).

To represent in a simple way the galaxies with $b > 1$ we have computed a set of models consisting of two short bursts separated by a time delay of 3 Gyr. The first burst has $\tau = 0.3, 5$ Gyr, the second burst $\tau = 0.3$ Gyr. In these clear examples most of the galaxy mass in stars ($> 70\%$) has been formed during the first burst but almost all of the current star formation activity is due to the second burst. In this way the UV flux is controlled by the current SFR while the red and IR fluxes are largely controlled by the stellar population formed in the past 3 Gyr during the first burst. Time delays greater than 3 Gyr have not been considered since they are hard to infer from the broad band spectral fits. Indeed, for values > 3 Gyr the shape of the red part of the galaxy spectrum does not change significantly.

This kind of star formation history can reproduce a current star formation activity greater than the average past rate, with a Scalo parameter in the range $b = 1 - 4$.

We have allowed for models based on different shapes (Scalo, Miller-Scalo or Salpeter) of the initial mass function (IMF) including stars in the $0.1 < M < 65 M_{\odot}$ range. We have also considered the case of metallicity $Z = Z_{\odot}$, $Z = 0.2Z_{\odot}$ and as low as $Z = 0.02Z_{\odot}$ since recent results on the spectral properties of the brighter $z \sim 0.5 - 1$ galaxies in the CFRS sample suggest the presence of non solar metallicities in a fraction $\sim 30\%$ (Hammer et al. 1997).

Two important features that alter the UV flux of high redshift galaxies must be added to the spectral synthesis models: the reddening produced by internal dust and Lyman series absorption produced by the neutral fraction of the intergalactic medium (IGM) intervening along the line-of-sight to each galaxy. While the former effect can be already appreciable at intermediate redshifts, the latter becomes important in the observed U,B,V bands only at $z > 2, 2.6, 3.5$ respectively.

We have adopted the attenuation law by Calzetti et

al. (1994,1997) which is derived from the observed local starburst galaxies and seems more appropriate when the absorption by the interstellar medium within each galaxy is clumpy, as expected in high z galaxies. This reddening curve is more grey than the Milky Way curve and does not show any 2000 Å bump.

For the Lyman series absorption produced by the IGM we have adopted the average HI opacity of a clumpy universe as a function of redshift computed by Madau (1995) where the average attenuation e.g. in the B band is ~ 1 mag at $z \sim 3.5$ and ~ 2 mag at $z \sim 4$.

Finally, at any redshift galaxies are allowed to have any age smaller than the Hubble time at that redshift ($\Omega = 1$ and $H_0 = 50 \text{ km s}^{-1}\text{Mpc}^{-1}$ have been adopted throughout the paper). A large dataset ($\simeq 10^6$) of “simulated galaxies” has thus been produced and compared with the observed colors. The full grid in the parameter space is shown in Tab. 2.

To show the main differences in the new GISSSEL library due to the different IMF and metallicities assumed, we have plotted in Fig. 1 various colors as a function of redshifts for a galaxy forming stars at a constant rate from $z = 5$ with metallicities $Z = 0.2, 1Z_{\odot}$ and assuming the Scalo or Salpeter IMFs. We note that the colors investigated here depend on the IMF rather than on metallicity for $0.1 \leq Z/Z_{\odot} \leq 1$. In particular, there are no appreciable changes in the $(R - I)_{AB}$ and $(V - I)_{AB}$ colors of $z > 2$ galaxies varying both metallicities and the IMF since the spectral shape for $\lambda < 4000 \text{ Å}$ rest-frame is similar at different metallicities. Differences in metallicity produce appreciable changes only in the $I_{AB} - K$ colors at $z < 1.5$. In contrast, $I_{AB} - K$ and $(B - I)_{AB}$ colors at a given $z < 1.5$ appear redder in the Scalo case.

The allowance for the presence of dust in the fitting models has some consequence on the estimated redshift distribution and on the cosmological evolution of the derived physical properties like the average SFR. In fact the presence of dust does not change appreciably the redshift estimate for $z < 1.4$ or $z > 2.8$ where we have strong color gradients due to the presence of the 4000 Å break or the Lyman absorption respectively. Nevertheless there is a specific redshift interval at $1.5 \leq z \leq 2.8$ where the expected dust free spectrum of any star forming galaxy is flat everywhere from the K down to the B band. Since the B band samples the 1500 Å rest frame region at $z = 2$, even a modest amount of dust ($E_{B-V} = 0.1$ in the rest frame) produces an appreciable reddening which shifts the dust-free redshift estimate from the true $z \sim 2$ toward the $z \leq 1.4$ region. Thus the inclusion of dust in the model computations reduces systematic errors present in

dust-free estimates of the photometric redshifts.

A general conclusion that can be drawn is that the selection of high z candidates ($z > 2.5$) does not depend strongly on the particular IMF or metallicity adopted, as discussed in Sect. 4. At $z < 1.5$ on the contrary, the photometry can provide information on the physical properties of the model, once the spectroscopic redshifts are known.

3.2. Statistical analysis

To obtain statistical information on the photometric redshifts of all the galaxies in the catalog we have applied a best-fitting procedure which is able to give the most appropriate spectral template matching the observed galaxy colors.

This “photometric redshift” approach is known to work successfully for low redshift bright galaxy samples where extensive calibration with spectroscopic redshifts is available (Sawicki et al. 1997, Lanzetta et al. 1997; see also Connolly et al 1995).

The classical χ^2 fitting procedure allows to take into account for redshift uncertainties due to photometric errors and to the similarity of model spectra at very different redshifts.

For each template we computed

$$\chi^2 = \sum_i \left[\frac{F_{observed,i} - s \cdot F_{template,i}}{\sigma_i} \right]^2 \quad (1)$$

where $F_{observed,i}$ is the flux observed in a given filter i , σ_i is its uncertainty, $F_{template,i}$ is the flux of the template in the same filter and the sum is over the 5 filters used in the field. The template fluxes have been normalized to the observed ones with the factor s .

When a given object is not detected in a particular filter because it is too faint we adopted the simple and conservative approach where all the models with theoretical fluxes below the flux limit are accepted, while the models with theoretical fluxes above the flux limit are weighted assuming that the flux observed is the flux limit. The best-fit redshift for each galaxy is reported in Tab. 1 together with its reduced χ^2_ν value. The redshift uncertainties ($z_{max} - z_{min}$ showing the 68% confidence interval) are obtained adopting the standard $\Delta\chi^2 = 1$ increment for the single parameter being estimated. In using the $\Delta\chi^2$ increment, a minimization with respect to the other parameters has been performed (Avni 1976). In this way, the resulting redshift uncertainties are obtained taking into account for both the photometric errors and the cosmic variance of the spectral templates.

The overall reliability of the method used is however given by the comparison between photometric and spectroscopic redshifts as shown in the next Section.

3.3. Calibrating photometric redshifts with the HDF galaxies

To assess the reliability of our technique we have compared photometric and spectroscopic redshifts available for 55 galaxies in the HDF for which infrared photometry is also available (Cowie 1997; Cohen et al. 1996; Dickinson 1998; Lowenthal et al. 1997). Our library of model spectra has been compared with this galaxy sample using the five HST bands UBV_{IK} for comparison with our five bands. Since an accurate determination of galaxy colors is essential to determine photometric redshifts with good accuracy, the galaxy magnitudes in the HDF have been re-estimated using the SExtractor package as in our field. Inspection of the HDF data shows that in selected cases, the presence of substructures or close pairs with different spectral characteristics is likely to affect the photometric accuracy of the redshift estimates. This is particularly true if the ground-based observations are taken in mediocre seeing conditions.

The calibration of the GISSEL models by means of spectroscopic redshifts for the HDF galaxies allows a better definition of the realistic space of the parameters involved. For a given IMF, the main parameters which should be controlled to avoid unrealistic model spectra are the dust reddening, age, metallicity and star-formation time-scale. Peculiar combinations of these parameters can introduce significant errors in the redshift estimates. This would be the case e.g. of models with a metallicity much less than the solar value but an old age of the galaxy and a substantial dust reddening. To be more specific, a trend between metallicity and age has been introduced where the case of extremely low metallicity ($Z = 0.02Z_\odot$) is restricted to very young galaxies, in general agreement with both observations and galaxy evolution models (e.g. Tantalo, Bressan & Chiosi 1997).

Moreover, a general correlation between metallicity and dust reddening has been introduced in the sense that young galaxies with low metallicity can be reddened only by a small amount of dust ($E_{B-V} \leq 0.05$). This trend has been discussed by Calzetti et al. (1994) as responsible for the correlation between the UV slope of the power-law continuum and the galaxy metallicity. In their sample, galaxies with low metallicities have a flatter UV spectrum on average, as expected if the dust reddening is lower.

Adopting this recipe based on reasonable constraints

supported by observations of nearby galaxies we have obtained for the average difference between spectroscopic and photometric redshifts in the HDF sample $\sigma_z \sim 0.1$ in the redshift interval $z = 0-3.5$ independently of the IMF. A value $\sigma_z \sim 0.2-0.3$ is obtained when the unconstrained overall spectral library is used.

The relations between photometric and spectroscopic redshifts are shown in Fig. 2 for all the IMF considered. As discussed above, an average $\sigma_z = 0.1$ (0.15) is found for galaxies with $z < 1.5$ ($z < 3.5$) independently of the IMFs. A small trend in the average $\langle \Delta z \rangle = \langle z_{spectr} - z_{phot} \rangle$ for galaxies with $z < 1.5$ has been observed depending on the IMF used. The Salpeter IMF shows an average underestimate by $\langle \Delta z \rangle = 0.09$ which reduces to $\langle \Delta z \rangle = 0.05$ for the Miller-Scalo IMF and to $\langle \Delta z \rangle = -0.04$ for the Scalo IMF. Thus the maximum difference in the photometric redshifts obtained by the different IMFs used is ~ 0.1 and an IMF shape steeper than a Salpeter one seems favoured by the GISSEL spectral models. In the next sections relevant results are given for the Miller-Scalo IMF.

As discussed in Sect. 3.1 the inclusion of dust does not change in general the discrimination between low ($z < 2$) and high ($z > 2$) redshift galaxies. In particular a typical decrease in the redshift estimate by $\Delta z \leq 0.2$ respect to the dust-free models is obtained for the high z HDF galaxies. The average amount of dust in the high redshift HDF galaxies with $z > 2$ depends of course on the IMF used. The Salpeter IMF produces a larger fraction of massive stars respect to the Scalo IMF and consequently a larger UV flux for a given star formation rate. Thus, at $z \sim 3$ a larger amount of dust is needed using the Salpeter IMF to reproduce the observed $U - K$ color. Average values of $E_{B-V} = 0.08, 0.11, 0.14$ are obtained for the Scalo, Miller-Scalo and Salpeter IMFs respectively.

The inclusion of the J, H bands allows a small improvement of the fit in the region $0.8 < z < 1.5$ with σ_z changing by a few thousandths. However a so small improvement could be due in part to the small number of galaxies with known spectroscopic redshifts in the $z = 1 - 2$ interval where the J band samples the 4000 \AA break.

In conclusion, GISSEL spectral models can provide photometric redshifts with comparable accuracy as obtained by means of the observed templates collected by Coleman, Wu, & Weedman (1980). Although different empirical approaches to derive photometric redshifts can provide better accuracy (Connolly et al. 1997), we have in this case the advantage to explore the spectral and physical properties of the galaxies derived from the GISSEL models.

This result is essentially due to the improvement of the new GISSEL library in the UV part of the model spectra (Bruzual & Charlot 1997) and to the inclusion of internal reddening by interstellar dust in galaxies and by the intergalactic neutral hydrogen absorption present along the line of sight.

4. GALAXIES AT VERY HIGH REDSHIFTS

As a first step we use the predicted spectral properties of the high redshift, star-forming galaxies to define a robust color selection for candidates in the redshift interval $3.8 < z < 4.4$. The bright fraction of these candidates represents an important sample for spectroscopic investigation. We then compare this method with the more sophisticated photometric redshift technique to check the robustness of the multicolor selection.

A very efficient method to select galaxies which are actively forming stars at high redshifts has been proposed by Steidel & Hamilton (1992). It is based on the detection of the Lyman break present in the flat rest-frame UV continuum of these galaxies. Steidel and Hamilton (1992) used a particular set of U G R filters to select the Lyman break galaxies in the redshift interval $2.8 < z < 3.4$. Since the spectrum of an actively star-forming dust-free galaxy is flat longward of the Lyman break, an average color of $G-R \sim 0.5$ is expected in the selected redshift interval. At the same time strong reddening is expected in the U-G color which samples the drop of the emission shortward of the Lyman break ($U-G > 1.5$) for $z \sim 3$ galaxies.

Steidel et al. (1996) confirmed with low resolution spectra at the Keck telescope the identification of the candidates in the expected redshift interval proving the high success rate ($> 70\%$) of this multicolor selection. Extrapolating the success rate obtained for the subsample of their candidates, they provided a first estimate of the surface density of galaxies at $z \sim 3$ of the order of 0.4 arcmin^{-2} .

Their UGR photometric system however limits the maximum redshift for the Lyman break galaxies to $z \simeq 3.5$. Indeed at higher redshifts the Lyman break enters the G band causing a reddening of the $G - R$ colors and an increasing contamination by low redshift galaxies.

4.1. The multicolor selection of the $3.8 < z < 4.5$ galaxies

To select galaxies at $z \sim 4$ it is better to sample the complex shape of the universal opacity to the UV photons of the intergalactic medium. We have plotted in Fig. 3 the spectrum of a dust-free galaxy forming stars

at a constant rate at $z = 3.25$ or $z = 4.25$ (Bruzual & Charlot 1997), including the average attenuation due to the IGM absorption (Madau 1995, Madau et al. 1996). It is clear that the most prominent spectral features come from the depression due to the average Lyman series absorption and from the cutoff at the continuum Lyman edge. While the Ly α forest absorption produces a fractional decrement of only $\sim 30\%$ at $z \simeq 3$, at $z \sim 4.5$ about 60–70% of the galaxy emission is lost causing a strong and easily detectable reddening at the blue frequencies.

An efficient sampling of this complex absorption requires at least four broad band filters in the optical range. We have chosen the Johnson BV , Gunn r and Kron-Cousin I filters, that are shown as broken lines in Fig. 3, superposed to the galaxy spectra.

In our natural AB photometric system described in Section 2 we expect high redshift, dust-free galaxies to show a marked flat spectrum through the r, I bands dominated by star-forming emission resulting in a $(R-I)_{AB} \simeq 0$ color. At the same time we expect an increasing reddening of the spectrum below 5500 Å for a $z \sim 4$ galaxy because of the IGM absorption. The corresponding colors will be large in $(V-I)_{AB}$ because of Ly α absorption and even larger in $(B-I)_{AB}$ colors when the flux in the B band is cut by Lyman continuum absorption (Fig. 3).

Thus high redshift galaxies appear well segregated in our color space (Fig. 1) independently of plausible ranges of the model parameters involved. The $(R-I)_{AB}$ color is sampling the intrinsic spectrum of galaxies in a wide redshift interval up to $z = 4.4$, where the IGM absorption in the r band begins to produce an appreciable reddening in the $(R-I)_{AB}$ color. Thus, in the redshift range $1.5 < z < 4.4$ all star-forming galaxies show $(R-I)_{AB} \sim 0 \pm 0.1$. On the other hand, IGM absorption produces strong reddening first in $(B-I)_{AB}$ ($(B-I)_{AB} > 1.4$ at $z > 3.5$), then in $(V-I)_{AB}$ ($(V-I)_{AB} > 0.7$ at $z > 4$). Thus, the simultaneous presence of the three colors at the average expected values can select star forming galaxies with small dust reddening at $z \geq 4$ (Fontana et al. 1996, Giallongo et al. 1996).

At $z < 1.5$ the $(R-I)_{AB}$ colors are sampling progressively longer rest-frame wavelengths, where the galaxy spectra are in general steeper, always resulting in $(R-I)_{AB} > 0.2$. Any possible contamination by an old population with steep blue spectra (a pronounced 4000 Å break) producing red $(B-I)_{AB}$ and $(V-I)_{AB}$ colors at $z = 0.5 - 1$ can be avoided just requiring a “flat” $(R-I)_{AB}$. The availability of deep K band photometry in the field helps to constrain even more the colors of $z \sim 4$ galaxies which would always have $I_{AB} - K < 2.5$

colors.

Taken all together, these results may be used to define relatively sharp color criteria that select high redshift galaxy candidates, similar to what was done by Steidel et al 1995 and Madau et al 1996. In our case, star forming galaxies in the redshift interval $3.8 \leq z \leq 4.4$ can be selected by imposing $(R-I)_{AB} \leq 0.1$, $(V-I)_{AB} \geq 0.5$, $(B-I)_{AB} \geq 2$. By adding the constraint on the $I_{AB} - K < 2$ color and allowing for $(R-I)_{AB} > 0.2$, galaxies at $z > 4.5$ can be selected.

Following this multicolor selection criterion we have identified 6 objects as star-forming galaxy candidates at $3.8 < z \leq 4.4$, taking into account upper limits in the B band. The spectroscopic follow-up of these objects is difficult even for 10m-class telescopes. At the typical magnitude and redshifts of our objects, the UV absorption lines fall in the spectral region affected by strong sky emission and can hardly be detected.

We stress here that even small amounts of dust can produce a systematic overestimate of the redshift for the $z > 3$ galaxies. As a result, a dust-reddened galaxy with $E_{B-V} \simeq 0.1$ at $z \sim 3$ can mimic typical colors of a dust-free galaxy at $z \sim 3.5$. For this reason it is difficult to evaluate from a selection in the color-color plane, the surface densities of the $z \sim 3$ and $z \sim 4$ galaxies, separately, and a more sophisticated best fitting procedure involving observed and predicted colors including dust reddening should be pursued as described in the next Section.

4.2. The photometric redshift distribution of galaxies up to $z \sim 4.5$

The photometric redshift distribution of the galaxies in our field is shown in Fig. 4. A peak in the redshift distribution is present at $z \sim 0.6$ with few galaxies at $z > 1.5$. This implies that at the magnitude limit for spectroscopic follow up ($R_{AB} \sim 25.5$), the bulk of the faint galaxies is at redshift $z < 1$ and any information about the luminosity function of galaxies at $z \geq 2$ can be obtained by means of large and deep surveys of galaxies having reliable photometric redshifts.

However, at variance with brighter surveys limited at $I < 22.5$ a tail in the z distribution appears for $z > 1.5$ and extending to $z \sim 4.5$. The broad band energy distributions of some of them are displayed in Fig. 5, together with the best-fitting spectrum. As it can be recognized, the high z identification is provided by the large $(B-I)_{AB}$ and $(V-I)_{AB}$ colors sampling the IGM absorption provided that $(R-I)_{AB}$ and $I_{AB} - K$ colors are consistent with the flat spectrum of a star-forming galaxy.

We find 8 galaxy candidates in our field at $2.8 \leq z \leq 3.5$ corresponding to a surface density of 1.6 arcmin^{-2} . This is 4 times larger than the recent estimates of Steidel et al. (1996) in the same redshift interval. Given the small area of our field (4.84 arcmin^2) fluctuations in the surface density of high redshift galaxies can explain this difference. Indeed our estimate is in good agreement with the number of spectroscopically confirmed galaxies found by Lowenthal et al. (1997) in the HDF at a similar depth $I_{AB} \leq 25.3$. They found 7 confirmed galaxies in the HDF. Thus the surface density of $z \sim 3$ galaxies with $R' \leq 25$ (or $I_{AB} \leq 25.3$) is about 1.6 arcmin^{-2} both in our field and in the HDF.

The derived surface density at $3.5 < z \leq 4.4$ in our field is lower. Indeed we find 5 of the 6 objects selected by our multicolor selection (see Sect. 4.1), one object being lost because was at the edge of our color selection. The surface density in this redshift interval is 1 arcmin^{-2} . In these estimates we have excluded the $z \sim 4.7$ galaxy companions discovered a few arcseconds away from the quasar (Hu, McMahon, & Egami 1996, Fontana et al. 1996, Petitjean et al. 1996).

One further high redshift candidate (#12 in our list) has been excluded from our statistical analysis. At the faint magnitude limit of our sample, compact, late type stars have colors which can mimic compact, high redshift galaxies. We have used a 150 m HST exposure of this field obtained for a different program by three of us (R.McM., E.H. and E.E.) to study the morphology of our high redshift candidates. Object #12 is the only one with a stellar appearance. A Keck spectrum obtained in the spring of 97 (Cowie and Hu, private communication) does not rule out the identification with a late star.

Indeed, late type stars can show colors similar to that expected from $z \sim 4$ galaxies. Moreover, the compact nature of the high redshift galaxies (Steidel et al. 1996) prevents any a priori exclusion of the high z candidates based mainly on their morphological compactness. Therefore some small contamination could be present in the $z \sim 4$ candidates. In our catalog however all the remaining $z > 3.5$ candidates are clearly extended.

Finally, our estimate is a lower limit if a significant fraction of $z > 4$ star-forming galaxies have their intrinsic UV emission strongly attenuated by dust extinction. Early type galaxies whose star formation has happened at even higher redshifts in a short burst are also missed in optical surveys. Very deep large field surveys in the K band ($K \sim 24$) are needed to provide an unbiased sample of high z galaxies.

5. THE DWARF POPULATION AT INTER-MEDIATE z

5.1. The luminosity function

To compare in more detail our results with other surveys we have computed the average volume density of galaxies with $19.5 < R' < 25$ derived in the redshift interval $0.5 < z < 0.75$ where we have sufficient statistics and where the redshift estimate is less uncertain due to the presence of the 4000 \AA break in the $V - R$ color. The luminosity function has been computed following Lilly et al. (1995) using the $1/V_{max}$ formalism: $\phi(M, z)dM = \sum_k 1/V_{max}$. Absolute rest frame blue AB magnitudes have been computed directly from the luminosities of the best-fit model spectra. These fluxes represent an interpolation between the observed $V' - R'$ colors at $z \sim 0.6$. Thus the spectral fit obtained for each galaxy provides the appropriate k-correction for each spectral type in the galaxy sample. The resulting luminosity function is shown in Fig. 6a in the magnitude interval $-20 < M_{B_{AB}} < -17$. For comparison we have plotted the analytical fit (dotted line) obtained in the same redshift interval by Lilly et al. in the CFRS sample at $I < 22.5$. Comparing our data with the CFRS data it appears that the luminosity function is consistent with the average density of brighter surveys like CFRS and Autofib/LDSS (Ellis et al. 1996) for $M_{B_{AB}} \leq -19.5$ while it shows a sharp steepening for magnitudes fainter than $M_{B_{AB}} = -19$. A density of $\sim 2 \times 10^{-2} \text{ Mpc}^{-3} \text{ mag}^{-1}$ at $M_{B_{AB}} = -17.5$ is reached, in general agreement with that derived in the HDF in about the same redshift interval by Sawicki et al. (1997).

Bringing together the CFRS and our luminosity functions results in a global LF which is not well represented by a Schechter shape since a steepening over the Schechter faint-end slope derived from the CFRS sample is apparent at $M_B > -19$ in our data. This steepening is reminiscent of that found in the local luminosity function by Zucca et al. (1997) where a similar volume density of the order of $2 \times 10^{-2} \text{ Mpc}^{-3} \text{ mag}^{-1}$ is obtained at magnitudes $\sim M_{B_{AB}} = -15$ (see Fig. 6b). We note that, with a dimming of 2 magnitudes, our LF is in good agreement with the local LF for $M_{B_{AB}} \geq -17$ within the rather large errors. Thus a strong luminosity evolution is suggested for the faint end of the luminosity function in the redshift range $z = 0 - 0.8$. Since it is known from brighter surveys that the luminosity evolution of L^* galaxies is small (cf. Ellis 97), a cosmological scenario where a different population of dwarf galaxies is subject to a strong luminosity evolution (Cowie et al. 1991, Babul & Rees

1992, Phillipps & Driver 1995) appears consistent with the LF evolution derived from this photometric sample. Although more complex scenarios involving number density evolution can not be excluded by the present data, larger and deeper photometric surveys are needed to constrain the evolution of the faint end of the galaxy LF.

5.2. The physical properties of galaxies at intermediate z

When the photometric estimate of the galaxy redshift is accurate (i.e. $\sigma_z \leq 0.1$) the best-fit model predicts intrinsic luminosities and related physical parameters like in particular age, star-formation rate and mass for each galaxy in the sample. The estimates of the luminous stellar mass are not unique because depend on crucial galaxy properties like the IMF adopted in the models. The ages derived by different authors differ by as much as 30% (e.g. Charlot 1996, Charlot, Worthey & Bressan 1996). In the framework of the models adopted here we have found that photometric uncertainties $\delta m \sim 0.1$ in the broad bands produce, at the best-fit redshift, uncertainties by a factor 2 in the previously mentioned physical parameters. Taking these uncertainties in mind we concentrate in identifying statistical trends suggested by the observations rather than in determining the true values of the physical parameters for each galaxy in the sample.

Fig. 7 shows the distribution of the galaxy ages in the redshift interval $z = 0.4 - 0.8$. The distribution has a median age of 10^9 yr. It is to note that flat spectrum, star-forming galaxies with $B' - I' \leq 1.4$ as defined in color surveys (Cowie et al. 1996), show a narrow distribution peaked at 2×10^8 yr testifying the presence of a population of very young star-forming galaxies.

Only a small fraction ($\sim 20\%$) of galaxies has been recognized with a signature in their broad band spectra of a recent episode of star formation superimposed to an older component (i.e. with a Scalo parameter $b > 1$). Most of these galaxies have $B' - I' > 1.4$. Although they show some current star-formation activity, most of their luminous stellar mass belongs to an older episode of star formation.

A second important parameter derived from our fitting technique is the mass in stars present in the galaxies. This is tied to the absolute magnitude in the K band, M_K , and it is relatively insensitive (within the accuracy previously discussed in this Section) to the accurate estimates of the galaxy age and metallicity. The stellar mass distribution for the galaxies in the redshift interval $z = 0.4 - 0.8$ where the LF has been computed, is shown in Fig. 8. The dis-

tribution of the mass has a median value $\sim 5 \times 10^8 M_\odot$. However the sample of the blue galaxies with $B' - I' \leq 1.4$ has a narrower distribution with a mean at $\sim 10^8 M_\odot$ and with no galaxies having $M > 2 \times 10^9 M_\odot$. This implies that the bulk of blue galaxies with $B' \sim 25$ has a very small luminous stellar mass.

In summary, considering the redshift distribution in Fig. 4 it appears that the majority of galaxies at $z < 1$ has a mass $M < 2 \times 10^9 M_\odot$ and an average age $\sim 10^9$ yr.

These results suggest that any pure luminosity model (PLE) based on a single formation redshift (usually confined $z > 2$) adopted for all the faint field galaxies is inconsistent with the short age and small mass determination of the blue redshift galaxies observed in the $z = 0.4 - 0.8$ redshift interval. Indeed the median formation redshift derived for these star forming galaxies is $z_{form} \simeq 0.9$.

6. THE STAR FORMATION HISTORY OF THE FIELD GALAXIES

The observed luminosity density at the rest frame $\lambda \sim 2800$ has been computed in each redshift bin as $\sum_i L_i / V_{max,i}$ with $V_{max,i}$ for each galaxy i defined as for the evaluation of the luminosity function. The cosmological trend in Fig. 9 and Tab. 3 shows an increase up to $\phi_{2800} = 2 \times 10^{19} \text{ W Hz}^{-1} \text{ Mpc}^{-3}$ at $z = 0.8 - 1$ and a gradual decline towards a value $\sim 10^{19} \text{ W Hz}^{-1} \text{ Mpc}^{-3}$ at $z \sim 3 - 4$.

We can also estimate the cosmological metal production rate directly from the observed luminosity density assuming dust free emission and solar metallicity, in analogy with previous similar estimates (e.g. Cowie et al. 1996; Madau et al. 1996, Connolly et al. 1997). The values are reported on the same Fig. 9.

It is to note that the values shown in Fig 9 represent the actual values measured in our samples. We have applied no correction to account for galaxies fainter than our magnitude limit in contrast with the values computed by Lilly et al. (1995), Madau et al. (1996), Sawicki et al. (1997), Connolly et al. (1997) where a correction for incompleteness by a factor 2.5 at $z \sim 1$ as derived from an extrapolation of the luminosity function has been applied to the CFRS data. In fact our values at $z = 0.4 - 0.6$ are in very good agreement with the observed values by Lilly et al. (1995) for galaxies with $I_{AB} \leq 22.5$. Our observations indicate that the contribution by fainter galaxies with $I_{AB} = 22.5 - 25$ is small in this redshift interval. The maximum value $\log \phi = 19.25$ at $z = 0.7 - 1$ is only

0.15 higher in our 2.5 mag fainter sample and in good agreement with the value $\log \phi = 19.3$ derived by Connolly et al. (1997) from the deeper HDF sample. Thus small corrections are expected in the $0.3 \leq z \leq 1$ interval with respect to the values plotted in Fig. 9. At $z = 1 - 2$ a comparison with the observed values derived from the HDF sample ($\log \phi \sim 19.5 - 19.4$; Connolly et al. 1997) suggests that our brighter sample provides a luminosity density a factor 2 lower (Fig. 9).

We have also included in Fig. 9 the recent local ($z \simeq 0.15$) data by Treyer et al. (1997) which update to a higher value the local UV emissivity. The local UV emissivity is provided by an UV galaxy luminosity function extended towards luminosities as low as the ones in the $z \sim 0.5 - 0.8$ blue LF. Adding this new local value it appears that the cosmological luminosity density changes by a factor ~ 2.5 in the overall redshift interval $z = 0.1 - 4$. This factor can increase to ~ 3.5 considering deeper results from the HDF. Thus any evidence of a marked maximum in the luminosity density at $z \sim 1 - 1.5$ appears blurred especially if we consider that at $z > 2$ we are sampling only bright galaxies with $L_B \geq L^*$ and corrections for the contribution by fainter galaxies become appreciable even in the HDF sample. A conservative estimate at $z = 3$ gives $\log \phi \sim 19.4$ (Madau 1997). A decline appears at $z > 3.5$ but the statistical uncertainties at these very high redshifts are large.

At this point, rather than converting the observed UV luminosity density in a star-formation rate by means of a fixed conversion factor, we have exploited the information derived from the best-fit, spectral models to compute the SFR in individual galaxies from their intrinsic dereddened colors.

The distribution of the star-formation rate per unit comoving volume as a function of redshift is shown in Fig. 10. The average mass density formation rate increases from the local value $\sim 0.025 M_\odot \text{ yr}^{-1} \text{ Mpc}^{-3}$ (for a Miller-Scalo IMF and $E_{B-V} = 0.1$) up to $\sim 0.05 M_\odot \text{ yr}^{-1} \text{ Mpc}^{-3}$ in the redshift interval $z = 0.75 - 1$. At redshift $z \sim 3$ there is a decline toward values $\sim 0.03 M_\odot \text{ yr}^{-1} \text{ Mpc}^{-3}$, 2 times lower than at $z = 0.75 - 1$ but comparable to the local value. At $z > 3.5$ the SFR decreases progressively. It is to note that the galaxy spectral models provide evidence for appreciable amount of dust reddening, increasing the SFR distribution by a factor 2.5 in the redshift interval $z = 0.6 - 1$ (corresponding to a typical $E_{B-V} \sim 0.1$ using the Calzetti attenuation law) respect to the value derived from the luminosity density evolution assuming no dust attenuation. On the other hand, only a relatively small fraction $\sim 25\%$ of the galaxies in the field

shows a color behaviour indicative of very low metallicity, with $Z < 0.1 Z_\odot$. These very blue galaxies provide an appreciable UV luminosity density but a corresponding SFR 1.4 smaller than expected from stars with $Z \simeq Z_\odot$. We note however that the fraction of galaxies showing very low metallicity depends on the assumed IMF and on the accurate photometry available from the B to the K band. This value should only be taken as indicative of the presence of a significant fraction of low-metallicity galaxies.

The same considerations done for the luminosity density evolution apply to the cosmological evolution of the average SFR. Any change in the SFR in our sample is confined within a factor ~ 2.5 in the redshift interval $z = 0.1 - 3.5$.

Finally, the cosmological evolution of the stellar mass per Mpc^3 in our sample increases for decreasing redshifts reaching a value $\sim 10^8 M_\odot \text{ Mpc}^{-3}$ at $z \sim 0.5$ (Fig. 11). This behaviour follows the cosmic evolution of the SFR per comoving volume. Considering the small age resulting for the galaxies with $z = 3 - 4$, the stellar mass density at very high redshifts is only 10–20% of that present at $z \sim 0.5$. On the other hand, the mass contribution at these very high redshifts predicted by models based on hierarchical clustering and merging is $\leq 7\%$ at $z \geq 3$ for the Miller-Scalo IMF (Baugh, Cole & Frenk 1996), a value smaller although not far from that derived from the observation. However, since incompleteness in the cosmological SFR (and correspondent stellar mass) at $z \sim 3 - 4$ by a factor ≥ 1.4 (Madau 1997) could be present, an increasing discrepancy with the values predicted by these models should be expected.

7. CONCLUSIONS

Photometric redshifts have been obtained from the $R' \leq 25$ galaxies selected in the field of the high redshift ($z = 4.7$) quasar BR 1202-0725. The wide spectral coverage obtained from deep BVR_{IK} multicolor photometry has allowed an accurate redshift estimate for each galaxy. This has been obtained comparing the observed colors with those predicted by spectral synthesis models including UV absorption by the IGM and dust reddening. We have discussed the accuracy of the method using a control sample of galaxies in the HDF with spectroscopically confirmed redshifts. The main conclusions can be summarized in the following items.

- A comparison between spectroscopic and photometric redshifts for a sample of galaxies selected in the

Hubble Deep Field has shown that spectral synthesis models (Bruzual & Charlot 1997) including UV absorption by the IGM and dust reddening can provide photometric redshifts with comparable accuracy ($\sigma_z \leq 0.1$ at $z \leq 1.5$) as obtained by means of the observed spectral templates of local galaxies. The present approach has the advantage to exploit the information on the spectral and physical properties derived from the GISSEL models for each galaxy in the sample. An IMF shape steeper than a Salpeter law provides unbiased redshift estimates and the following statistical results are given for a Miller-Scalo IMF.

- The redshift distribution of the $R' \leq 25$ galaxies is peaked at $z = 0.6$ with 16% of the sample at $z > 1.5$. The derived surface density of the $z \sim 2.8 - 3.5$ galaxies having $\langle M_{B_{AB}} \rangle = -21$ in our field is 1.6 arcmin^{-2} in agreement with that derived in the HDF (1.5 arcmin^{-2}) at about the same magnitude. This corresponds to a comoving volume density of 10^{-3} Mpc^{-3} similar to the local density of galaxies with the same luminosities. The derived surface density at $3.5 < z \leq 4.5$ in our field is lower, 1 arcmin^{-2} .
- The estimated luminosity function at $z \sim 0.6$ shows a strong steepening for $M_{B_{AB}} > -19$ with respect to the extrapolation derived from brighter redshift surveys. A comoving volume density of $2 \times 10^{-2} \text{ Mpc}^{-3}$ at $M_{B_{AB}} = -17.5$ is obtained. Comparing with the local luminosity function, a luminosity evolution by about 2 magnitudes is suggested for galaxies with $M_{B_{AB}} > -19$.
- The bulk of the intermediate redshift population mostly consists of very young star-forming galaxies with a median age $\leq 10^9 \text{ yr}$ and a small stellar mass $M \sim 5 \times 10^8 M_\odot$. In particular, the blue fraction with $B' - I' < 1.4$ shows a median age of $2 \times 10^8 \text{ yr}$ and stellar mass $M \sim 2 \times 10^8 M_\odot$. Any pure luminosity model (PLE) based on a single formation redshift (usually confined to $z > 2$) adopted for all the faint field galaxies appears inconsistent with these small age and mass evaluations.
- The observed 2800 \AA luminosity density and the associated star formation rate in our sample show an increase to $\phi \sim 2 \times 10^{19} \text{ W Hz}^{-1} \text{ Mpc}^{-3}$ (or $SFR \sim 5 \times 10^{-2} M_\odot \text{ yr}^{-1} \text{ Mpc}^{-3}$) at $z \sim 0.8$, i.e. only by a factor 2.5 larger than the local value.

At $z > 1$ the UV luminosity density and the corresponding SFR decrease to values comparable to the local one. Thus evidence of a marked maximum in the luminosity density and SFR at $z \sim 1$ appears blurred especially if we consider that an significant corrections for fainter undetected galaxies are expected at $z > 1$. A comparison between the average cosmological luminosity density and the corresponding star formation rate at $z = 0.4 - 1$ implies an average $E_{B-V} \simeq 0.1$, adopting the Calzetti (1997) attenuation law and a Miller-Scalo IMF. Finally, the derived cosmological mass in luminous stars per comoving volume at $z \sim 3 - 4$ is $\sim 20 - 10\%$ of that formed at $z = 0.5$, a value larger although not far from that predicted by the standard hierarchical clustering scenario.

We thank S. Charlot for providing the most recent version of the GISSEL library and for comments on an early version of the paper, S. Arnouts for help in computing magnitudes for the HDF galaxies, E. Zucca for providing data in advance of publication and A. Renzini for useful discussions. This work was partially supported by the ASI contract 95-RS-38 and by the Formation and Evolution of Galaxies network set up by the European Commission under contract ERB FMRX-CT96-086 of its TMR programme.

REFERENCES

- Avni, Y., 1976, ApJ, 210, 642
- Babul, A., & Rees, M., 1992, MNRAS 255, 346
- Baugh, C. M., Cole, S., & Frenk, C. S., 1996, MNRAS 282, L27
- Bertin, E., Arnouts, S. 1996, A&AS, 117, 393
- Bruzual, G., & Charlot, S., 1993, ApJ, 405, 538
- Bruzual, G., & Charlot, S., 1997, in preparation
- Calzetti, D. 1997, in "The Ultraviolet Universe at Low and High Redshift", in press, astro-ph/9706121
- Calzetti, D., Kinney, A. L., Storchi-Bregmann, T. 1994, ApJ, 429, 582
- Charlot, S. 1996 in From Stars to Galaxies, ed. Leitherer, C. & Fritze, U., Huchra, J. (ASP Conference Series), p. 275
- Charlot, S., Worthey, G., & Bressan, A. 1996, ApJ 457, 625

- Cohen, J. G., et al., 1996, ApJ, 471, L1
- Cole, E., Aragón-Salamanca, A., Frenk, C. S., Navarro, J. F., Zepf, S. E. 1994, MNRAS, 271, 781
- Coleman, G. D., Wu, C-C, & Weedman, D. W. 1980, ApJS, 43, 393
- Connolly, A.J., Csabai, I., Szalay, A.S., Koo, D.C., Kron, R.G., 1995, AJ, 110, 2655
- Connolly, A. J., Szalay, A. S., Dickinson, M., SubbaRao, M. U., & Brunner, R. J. 1997, ApJ, 486, L11
- Cowie, L. L. 1997, <http://www.ifa.hawaii.edu/cowie/tts/tts.html>
- Cowie, L. L., Hu, E. M., Songaila, A. 1995, Nature, 377, 603
- Cowie, L. L., Songaila, A., Hu, E. M. 1991, Nature, 354, 460
- Cowie, L. L., Songaila, A., Hu, E. M., Cohen, J. G., 1996, AJ, 112, 839
- Dickinson, M. 1998, to be published in the proceedings of the STScI May 1997 Symposium “The Hubble Deep Field,” eds. M. Livio, S.M. Fall and P. Madau, astro-ph/9802064
- D’Odorico et al., 1996, in “HST and the High Redshift Universe”, Cambridge University Press
- Djorgovski S.G., 1995, in *Science with the VLT*, ed Walsh, Danziger
- Ellis, R. S. 1997, ARAA, 35, 389
- Ellis, R. S., Colless, M., Broadhurst, T. J., Heyl, J. S., Glazebrook, K. 1996, MNRAS, 280, 235
- Fall, S. M., Pei, Y. C., McMahon, R. G. 1989, ApJ, 341, L5
- Fontana, A., Cristiani, S., D’Odorico, S., Giallongo, E., Savaglio, S. 1996, MNRAS, 279, L27
- Francis et al, 1996, ApJ, 457, 460
- Gallego, J., Zamorano, J., Aragón-Salamanca, A., Rego, M. 1995, ApJ, 455, L1
- Giallongo, E., Charlot, S., Cristiani, S., D’Odorico S., Fontana A., 1996, in “The VLT and the high redshift Universe”, eds. Bergeron, p. 208
- Gwyn, S. D. J., & Hartwick, F. D. A. 1996, ApJ 468, L77
- Hammer et al. 1997, ApJ, 481, 49
- Hu, E. M., McMahon, R. G. 1996, Nature, 382, 231
- Hu, E. M., McMahon, R. G., Egami, E. 1996, ApJ, 459, L53
- Kennicutt, R. C., Tamblyn, P., & Congdon, C. W. 1994, ApJ, 435, 22
- Koo, D. 1985, AJ, 90, 418
- Koo, D., & Kron, R. G. 1992, ARAA, 30, 613
- Lanzetta, K. M., Yahil, A., Fernandez-Soto, A. 1996, Nature, 381, 759
- Lanzetta, K. M., Fernandez-Soto, A., Yahil, A. 1997, to be published in the proceedings of the STScI May 1997 Symposium “The Hubble Deep Field”, eds. M. Livio, S.M. Fall and P. Madau, astro-ph/9709166
- Lilly, S. J., Tresse, L., Hammer, F., Crampton, D., Le Fèvre, O., 1995, ApJ, 455, 108
- Lilly, S. J., Le Fèvre, O., Hammer, F., Crampton, D., 1996, ApJ, 460, L1
- Lowenthal, J. D., et al. 1997, ApJ submitted
- Macchetto, F. D., Lipari, S., Giavalisco, M., Turnshek, D. A., Sparks, W. B., 1993, ApJ, 404, 511
- Madau, P. 1995, ApJ, 441, 18
- Madau, P. 1997, in *Star Formation Near and Far*, in press
- Madau, P., Ferguson, H.C, Dickinson, M.E., Giavalisco, M., Steidel, C.C., Fruchter, A., 1996, MNRAS, 283, 1388
- McMahon, R. G., Omont, A., Bergeron, J., Kreysa, E., Haslam, C. G. T. 1994, MNRAS, 267, L9
- Pascarelle, S.M., Windhorst, R.A., Keel, W.C., Odewahn, S.C. 1996, Nature, 383, 45
- Petitjean, P., Peñontal, E., Valls-Gabaud, D., Charlot, S. 1996, Nature 380, 411
- Phillipps, S., & Driver, S. 1995 MNRAS, 274, 832
- Sawicki, M.J., Lin, H., Yee, H.K.C. 1997, AJ, 113, 1
- Songaila, A., Cowie, L. L., Hu, E., Gardner, J. P. 1994, ApJS, 94, 461
- Smail, I., Hogg, D. W., Yan, L., Cohen, J. G. 1995, ApJ, 449, L105
- Steidel, C. C., Hamilton, D., 1992, AJ, 104, 941
- Steidel, C. C., Pettini, M., Hamilton, D., 1995, AJ, 110, 2519
- Steidel, C. C., Giavalisco, M., Pettini, M., Dickinson, M., Adelberger, K. L. 1996, ApJ, 462, L17
- Thompson, D., Djorgovski, S., Trauger, J., 1995, AJ, 110, 963
- Treyer, M. A., Ellis, R. S., Milliard, B., Donas J., 1997, in *The Ultraviolet Universe at Low and High Redshift*. W.H. Waller ed. AIP in press

Warren, S.J. & Møller, P., 1996, A&A, 311, 25

Williams, R. E. et al. 1996, AJ, 112, 1335

Zucca, E., et al. 1997, A&A, 326, 477

FIGURE CAPTIONS

Fig. 1 Colors as a function of redshift for a galaxy forming stars at a constant rate from $z = 5$. Circles, triangles, squares and exagons are for $I - K$, $B - I$, $V - I$, $R - I$ AB colors, respectively. (Upper panel) Filled symbols are for a galaxy with metallicity $Z = 0.2Z_{\odot}$, open symbols for a galaxy with $Z = Z_{\odot}$. A Scalo IMF has been adopted. (Lower panel) Filled symbols are for a galaxy with the Salpeter IMF, open symbols for the Scalo IMF.

Fig. 2 Photometric redshift estimates versus spectroscopic redshifts for a subsample of galaxies in the Hubble Deep Field with K band photometry. Three different IMF have been adopted as shown in the Figure.

Fig. 3 The spectrum of a galaxy forming stars at a constant rate at $z = 3.25$ or $z = 4.25$. The average attenuation due to the IGM absorption is included. The Johnson BV , Gunn r and Kron-Cousin I filters are shown as broken lines.

Fig. 4 The photometric redshift distribution in our sample. Thick histogram shows the z distribution of galaxies with masses greater than $2 \times 10^9 M_{\odot}$.

Fig. 5 Examples of broad band energy distributions of high and intermediate redshift galaxies. The best-fitting spectrum is also shown.

Fig. 6 a) The luminosity function of our sample in the redshift interval $0.45 \leq z \leq 0.75$ and in the magnitude interval $-20 < M_{B_{AB}} < -17$. For comparison the analytical fit (dotted line) obtained in the same redshift interval by Lilly et al. (1996) at $I < 22.5$ is also shown. b) The same luminosity function shifted by 2 magnitude lower. The local luminosity function by Zucca et al. (1997) is also shown as empty circles. Their magnitudes have been scaled to $H_o = 50 \text{ km s}^{-1} \text{ Mpc}^{-3}$ and to the AB system ($B_{AB} = B - 0.16$).

Fig. 7 The distribution of galaxy ages in the redshift interval $z = 0.4 - 0.8$. Thick histogram shows the distribution of the blue, star forming galaxies with $B' - I' \leq 1.4$.

Fig. 8 The mass distribution in the redshift interval $z = 0.4 - 0.8$. Thick histogram shows the distribution of the blue galaxies with $B' - I' < 1.4$.

Fig. 9 The luminosity density distribution derived from our sample at the rest frame wavelength of 2800 \AA . The local value (filled circle) has been taken from Treyer et al. (1997). The directly observed values from the CFRS sample by Lilly et al. (1996) and from the HDF sample by Connolly et al. (1997) are shown as crosses and empty circles, respectively. The values derived from the $z > 2$ HDF sample (at $\lambda = 1500 \text{ \AA}$) by Madau et al. (1996) are also shown as empty squares. All these values have been converted in metal production rates (MPR) adopting the conversion factor as in Connolly et al. (1997).

Fig. 10 The distribution of the star-formation rate per unit comoving volume as a function of redshift for a Miller-Scalo IMF. The cross at $z = 0$ indicates the local value derived by Gallego et al. (1995).

Fig. 11 The cosmological evolution of the total formed mass in stars per unit comoving volume.